R-loops at centromeric chromatin contribute to defects in kinetochore integrity and chromosomal instability in budding yeast

Prashant K. Mishra[a], Arijita Chakraborty[b], Elaine Yeh[c], Wenyi Feng[b,*], Kerry S. Bloom[c], and Munira A. Basrai[a,*]

[a]Genetics Branch, Center for Cancer Research, National Cancer Institute, National Institutes of Health, Bethesda, MD 20892; [b]SUNY Upstate Medical University, Syracuse, NY 13210; [c]Department of Biology, University of North Carolina, Chapel Hill, NC 27599

ABSTRACT **R-loops, the byproduct of DNA–RNA hybridization and the displaced single-stranded DNA (ssDNA), have been identified in bacteria, yeasts, and other eukaryotic organisms. The persistent presence of R-loops contributes to defects in DNA replication and repair, gene expression, and genomic integrity. R-loops have not been detected at centromeric (*CEN*) chromatin in wild-type budding yeast. Here we used an *hpr1*Δ strain that accumulates R-loops to investigate the consequences of R-loops at *CEN* chromatin and chromosome segregation. We show that Hpr1 interacts with the *CEN*-histone H3 variant, Cse4, and prevents the accumulation of R-loops at *CEN* chromatin for chromosomal stability. DNA–RNA immunoprecipitation (DRIP) analysis showed an accumulation of R-loops at *CEN* chromatin that was reduced by overexpression of *RNH1* in *hpr1*Δ strains. Increased levels of ssDNA, reduced levels of Cse4 and its assembly factor Scm3, and mislocalization of histone H3 at *CEN* chromatin were observed in *hpr1*Δ strains. We determined that accumulation of R-loops at *CEN* chromatin contributes to defects in kinetochore biorientation and chromosomal instability (CIN) and these phenotypes are suppressed by *RNH1* overexpression in *hpr1*Δ strains. In summary, our studies provide mechanistic insights into how accumulation of R-loops at *CEN* contributes to defects in kinetochore integrity and CIN.**

Monitoring Editor
Daniel Lew
Duke University

Received: Jun 12, 2020
Revised: Oct 2, 2020
Accepted: Oct 29, 2020

INTRODUCTION

Faithful chromosome segregation is important for proper growth and development because chromosomal instability (CIN) leads to aneuploidy, which is a hallmark of many cancers and a significant driver of tumorigenesis (Bakhoum and Swanton, 2014; Barra and Fachinetti, 2018). The kinetochore, which includes centromeric (*CEN*) DNA, evolutionarily conserved protein complexes, and a defined chromatin structure, is essential for faithful chromosome segregation (Diaz-Ingelmo *et al.*, 2015; Bloom and Costanzo, 2017; Lawrimore and Bloom, 2019). The nucleotide composition and size of *CEN* range from ~125 base pairs of DNA in budding yeast point centromeres to megabases of complex ordered arrays of DNA repeats, termed as regional centromeres, in other eukaryotes (McKinley and Cheeseman, 2016; Bloom and Costanzo, 2017). Despite the differences in *CEN* DNA, *CEN* identity is marked epigenetically by an evolutionarily conserved *CEN*-specific histone H3 variant (Cse4 in budding yeast, Cid in flies, CENP-A in humans) (Heun *et al.*, 2006; McKinley and Cheeseman, 2016; Mishra and Basrai, 2019; Sharma *et al.*, 2019). The recruitment of Cse4 to the *CEN* chromatin is mediated by a Cse4-specific assembly factor, Scm3 (HJURP in humans) (Camahort *et al.*, 2007; Mizuguchi *et al.*, 2007; Stoler *et al.*, 2007). The *CEN* incorporation of Cse4 mediates the assembly of conserved kinetochore protein complexes, resulting in a highly ordered, unique, topologically distinct configuration of *CEN* chromatin, which is essential for faithful chromosome segregation (Mishra *et al.*, 2013; Diaz-Ingelmo *et al.*, 2015; Bloom and Costanzo, 2017;

This article was published online ahead of print in MBoC in Press (http://www.molbiolcell.org/cgi/doi/10.1091/mbc.E20-06-0379) on November 4, 2020.

*Address correspondence to: Munira A. Basrai (basraim@nih.gov) or Wenyi Feng (fengw@upstate.edu).

Abbreviations used: C-loop, centromere loop; CEN, centromere; CF, chromosome fragment; ChIP, chromatin immunoprecipitation; CIN, chromosomal instability; DRIP, DNA-RNA immunoprecipitation; FACS, fluorescence-activated cell sorting; GFP, green fluorescent protein; IP, immunoprecipitation; KT-MT, kinetochore-microtubule; lncRNA, long non-coding RNA; ORF, open reading frame; qPCR, quantitative PCR; RNAPII, RNA polymerase II; SPB, spindle pole body; ssDNA, single-strand DNA.

Lawrimore *et al.*, 2018). Notably, the structural integrity and topological organization of *CEN* chromatin is an active area of research. For example, the formation of *CEN* loops, termed as C-loops (Bloom and Costanzo, 2017), is essential for the separation of sister *CEN*s and kinetochore assembly in the absence of the Ctf19, Okp1, Mcm21, Ame1 (COMA) complex (Lawrimore *et al.*, 2018; Lawrimore and Bloom, 2019). The dynamic configuration of *CEN* C-loops facilitates kinetochore biorientation for faithful chromosome segregation (Yeh *et al.*, 2008; Lawrimore and Bloom, 2019). Moreover, under- and/or overwinding of DNA, referred to as DNA supercoiling, also regulates the topology of *CEN* chromatin (Furuyama and Henikoff, 2009; Henikoff and Furuyama, 2010). Notably, in vitro studies have shown that *CEN* DNA is positively supercoiled, and this configuration is mediated by Cse4 and Cid in budding yeast and flies, respectively (Furuyama and Henikoff, 2009; Huang *et al.*, 2011). We have shown that the evolutionarily conserved protein Pat1 (PATL1 in humans) associates with *CEN* chromatin and regulates Cse4 levels and DNA supercoiling at *CEN* chromatin in vivo (Lawrimore *et al.*, 2011; Haase *et al.*, 2013; Mishra *et al.*, 2013). The increase in the number of negative supercoils at *CEN* DNA contributes to errors in chromosome segregation in *pat1*Δ strains (Mishra *et al.*, 2013, 2015), suggesting that positive supercoiling of *CEN* DNA is important for chromosome stability.

In addition to C-loops and DNA supercoiling, R-loops are a structural feature of DNA topology that has important roles in gene expression, DNA replication, DNA damage and repair, and genomic integrity (Santos-Pereira and Aguilera, 2015; Costantino and Koshland, 2018; Allison and Wang, 2019). R-loops are transcriptional byproducts, representing a three-stranded nucleic acid structure that contains a DNA–RNA hybrid and a displaced DNA strand (Santos-Pereira and Aguilera, 2015; Allison and Wang, 2019). R-loops are evolutionarily conserved nucleic acid structures and have been observed in bacteria, yeasts, and other eukaryotic organisms (Santos-Pereira and Aguilera, 2015; Allison and Wang, 2019). R-loops are preferentially enriched at highly expressed regions peaking at RNA polymerase II (RNAPII) start and end sites (Rondon and Aguilera, 2019). Accumulation of R-loops has been shown to be deleterious for genomic integrity as they act as physical barriers, which block the progression of replication forks, leading to DNA damage and genomic instability (Gan *et al.*, 2011; Santos-Pereira and Aguilera, 2015; Costantino and Koshland, 2018; Allison and Wang, 2019; Crossley *et al.*, 2019). Moreover, the displaced DNA strand in the R-loop is prone to DNA damage that predisposes cells to accumulate harmful mutations. If left unrepaired, these DNA mutations have been proposed to contribute to human diseases, including cancers (Groh and Gromak, 2014; Wells *et al.*, 2019). R-loops have also been shown to promote RNAPII-mediated transcription of antisense long noncoding RNAs (lncRNAs) in human cells (Rondon and Aguilera, 2019; Tan-Wong *et al.*, 2019) and facilitate efficient mRNA splicing of the second exon of the RPL28 gene in budding yeast (El Hage *et al.*, 2014).

Recent studies have identified RNAPII-mediated *CEN* transcription in the form of lncRNAs in both sense and antisense orientations in budding yeast (Chen *et al.*, 2019; Ling and Yuen, 2019). *CEN* lncRNA was detected in a wild-type (WT) strain arrested in S-phase of the cell cycle; increased *CEN* lncRNA was reported in *cbf1*Δ and *htz1*Δ strains when compared with a WT strain (Chen *et al.*, 2019; Ling and Yuen, 2019). However, R-loops have not been detected at *CEN* chromatin in WT budding yeast, even though they are enriched at ribosomal DNA, retrotransposons, telomeres, and open reading frames (ORFs) (~1490) that are transcribed primarily by RNAPII (Stirling *et al.*, 2012; Chan *et al.*, 2014; Costantino and Koshland, 2018). A genome-wide study for phosphorylation of histone H3 serine 10 (H3S10P) showed higher levels of H3S10P at ORFs, *CEN*s, peri-*CEN*s, and autonomously replicating sequence (ARS) regions in an *hpr1*Δ strain (Castellano-Pozo *et al.*, 2013). DNA–RNA immunoprecipitation (DRIP) analysis showed that higher levels of H3S10P correlate with R-loops in budding yeast, *Caenorhabditis elegans*, and human cells (Castellano-Pozo *et al.*, 2013). These studies confirmed the accumulation of R-loops at one of the *CEN*s, namely *CEN6* in cells arrested in G1-phase of the cell cycle in *hpr1*Δ strains (Castellano-Pozo *et al.*, 2013). Hpr1, a component of the THO/TREX complex, regulates genomic integrity (Aguilera and Klein, 1990; Chavez and Aguilera, 1997; Luna *et al.*, 2019). Increased DNA recombination, defects in mRNA export, and impairment of transcription elongation in the presence of the transcription elongation inhibitor 6-azauracil were observed in *hpr1*Δ strains (Fan *et al.*, 1996; Chavez and Aguilera, 1997; Chavez *et al.*, 2000; Zenklusen *et al.*, 2002; Huertas *et al.*, 2006). However, physiological consequences due to the accumulation of R-loops at *CEN* chromatin and its impact on kinetochore function have not been examined.

In this study, we show that accumulation of R-loops at *CEN* chromatin contributes to defects in the kinetochore integrity and CIN. Our results showed that Hpr1 interacts in vivo with Cse4 and that *hpr1*Δ causes accumulation of R-loops at *CEN* chromatin, correlating with increased single-stranded DNA (ssDNA) at *CEN*s and reduced levels of Cse4 and its assembly factor Scm3 with a concomitant increase in histone H3 at *CEN*s. We found that accumulation of R-loops at *CEN* chromatin contributes to defects in biorientation of sister chromatids during mitosis and increased frequency of chromosome loss in *hpr1*Δ strains, which were suppressed by *RNH1* overexpression. In summary, our results show that persistence of R-loops at *CEN* chromatin contributes to defects in the kinetochore integrity, resulting in CIN.

RESULTS

Hpr1 associates with centromeric histone H3 variant Cse4

Hpr1 was detected in a high throughput affinity screen for proteins that interact with overexpressed Cse4^{16KR} (all lysines mutated to arginine) (Ranjitkar *et al.*, 2010), which is highly stable and mislocalizes to non-*CEN* regions, leading to CIN (Au *et al.*, 2008). We examined whether Hpr1 interacts with Cse4 in vivo using immunoprecipitation (IP) experiments with a WT strain that expresses HA-tagged Hpr1 and Myc-tagged Cse4 from their native promoters at the endogenous locus. The HA tag does not affect the function of Hpr1 as this strain does not exhibit a temperature-sensitive growth defect observed in a *hpr1*Δ strain (Supplemental Figure S1). We first examined whether the expression of Hpr1 is cell cycle regulated by Western blot analysis of extracts prepared from an Hpr1-HA strain grown to logarithmic phase, arrested in G1 with α-factor, in S-phase with hydroxyurea (HU), or in G2/M with nocodazole (NOC). Fluorescence activated cell sorting (FACS) examination of nuclear position and cell morphology confirmed the synchronization of cells in these cell cycle stages (Figure 1, A and B). Our results showed that the expression of Hpr1 is not significantly affected by the cell cycle stage (Figure 1, C and D). We next examined whether Hpr1 interacts with Cse4 by performing IP experiments in which protein extracts from logarithmically growing cultures were incubated with agarose beads conjugated with anti-HA (Hpr1) and anti-Myc (Cse4) antibodies. No signals were detected in control experiments performed using a Cse4-Myc strain without Hpr1-HA. We observed an interaction between Hpr1 and Cse4 in a Cse4-Myc strain carrying Hpr1-HA (Figure 1E). On the basis of these results, we conclude that Hpr1 interacts in vivo with Cse4 under normal physiological conditions.

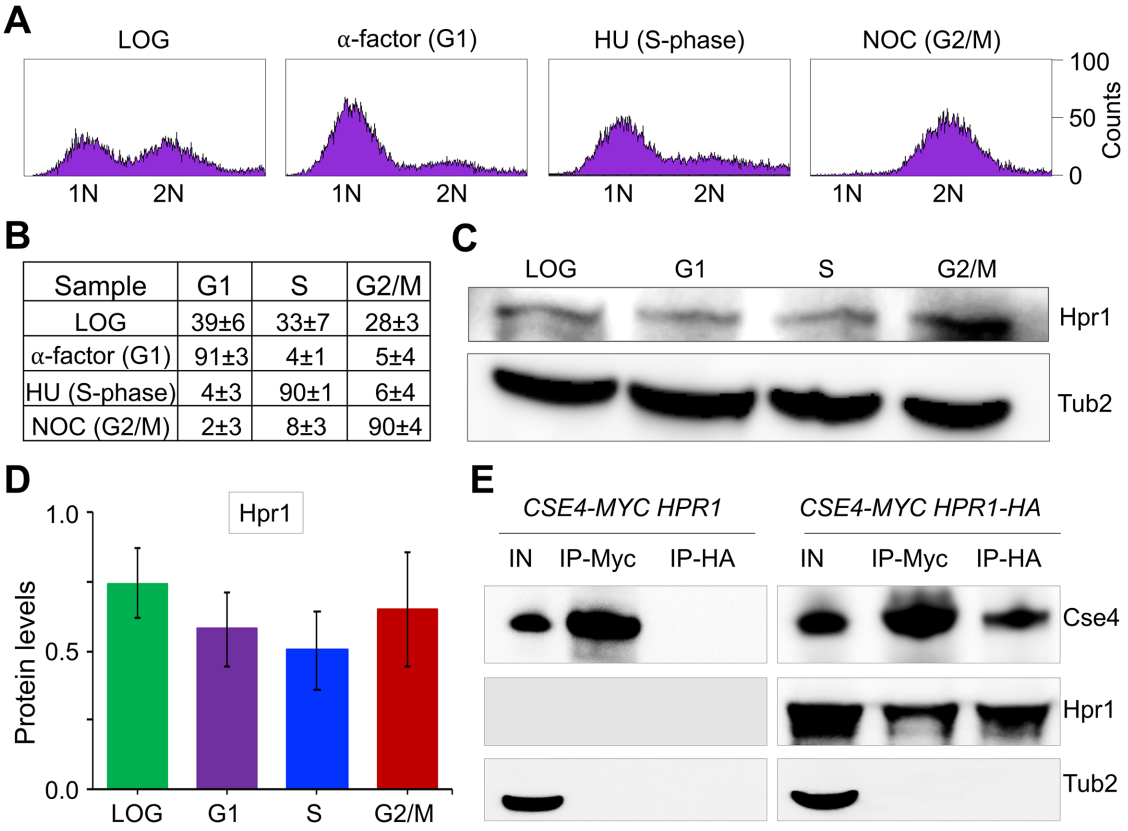

Sample	G1	S	G2/M
LOG	39±6	33±7	28±3
α-factor (G1)	91±3	4±1	5±4
HU (S-phase)	4±3	90±1	6±4
NOC (G2/M)	2±3	8±3	90±4

FIGURE 1: Hpr1 is expressed throughout the cell cycle and interacts with Cse4 in vivo. (A) FACS profile of WT (YMB11085, *CSE4-12MYC, HPR1-3HA*) cells grown in YPD to logarithmic (LOG) phase at 30°C and synchronized in G1 with α-factor, S-phase with HU and G2/M with nocodazole. (B) Cell cycle categorization of samples from A representing the percentage of cells in G1, S, and G2/M. (C) Western blots showing expression of Hpr1 and Tub2 (loading control). (D) Hpr1 expressed throughout the cell cycle. Protein levels of Hpr1 in LOG-, G1-, S-, and G2/M-phases of the cell cycle. Values were normalized to Tub2. Average from three biological replicates ± SE. (E) Hpr1 interacts in vivo with Cse4. WT strains YMB11085 (*CSE4-12MYC, HPR1-3HA*) and JG595 (*CSE4-12MYC, HPR1*) were grown in YPD at 30°C to the logarithmic phase. Cell extracts were prepared, and IPs were performed using anti-HA (A2095; Sigma-Aldrich) and anti-Myc (A7470; Sigma Aldrich) agarose beads. Eluted proteins were analyzed by Western blotting with anti-Myc (Cse4; a-14, sc-789; Santa Cruz Biotechnology), anti-HA (Hpr1; H6908; Sigma Aldrich), and anti-Tub2 (loading control) antibodies. IN = input, and IP = immunoprecipitated samples.

Hpr1 prevents the accumulation of R-loops at *CEN* chromatin

Our results for the interaction of Hpr1 with Cse4 prompted us to examine the role of Hpr1 in preventing the accumulation of R-loops at *CEN*s. We performed three independent experiments to assay the presence of R-loops at *CEN*s in WT and *hpr1*Δ strains. In the first experiment, we performed DRIP analysis using DNA from logarithmically grown WT and *hpr1*Δ strains with anti-DNA–RNA hybrid (S9.6) antibodies. FACS, nuclear position, and cell morphology analyses showed similar cell cycle profiles of WT and *hpr1*Δ strains (Figure 2, A and B). DRIP experiments were performed as described previously (Castellano-Pozo *et al.*, 2013; Costantino and Koshland, 2018; Kabeche *et al.*, 2018) followed by quantitative PCR (qPCR) to determine the levels of R-loops at the *CEN*s (*CEN1* and *CEN3*). R-loop–negative (179K) and –positive (169K) DNA regions identified in previous studies (Costantino and Koshland, 2018) were used as controls. DRIP–qPCR showed a significant accumulation of R-loops at *CEN1* and *CEN3* in an *hpr1*Δ strain when compared with that observed in the WT strain (Figure 2C). The accumulation of R-loops at the *CEN* chromatin is linked to the deletion of *HPR1* because the *hpr1*Δ strain transformed with plasmid-based *HPR1* resulted in a significant reduction in R-loops at *CEN1* and *CEN3*, the levels of which were similar to those observed in a WT strain (Figure 2C). No significant accumulation of R-loops was detected at the negative control 179K region, whereas significant accumulation of R-loops was detected at the positive control 169K region in WT and *hpr1*Δ strains (Figure 2C).

In the second experiment, we performed DRIP analysis after treatment of DNA with the ribonuclease RNase-H, which hydrolyzes RNA in DNA–RNA hybrids, leading to elimination of R-loops (Allison and Wang, 2019). No detectable R-loops were observed at *CEN1*, *CEN3*, or the negative control region (179K) with or without RNase-H treatment in a WT strain (Figure 2D). However, the accumulation of R-loops at *CEN1* and *CEN3* was reduced significantly upon treatment with RNase-H in a *hpr1*Δ strain (Figure 2D). As expected, R-loops at the positive control region (169K) were not detected after treatment with RNase-H in WT and *hpr1*Δ strains (Figure 2D).

In the third experiment, we assayed R-loops in WT and *hpr1*Δ strains overexpressing *RNH1*, which specifically eliminates the RNA strand of an DNA–RNA hybrid, resulting in the degradation of the R-loops (Huertas and Aguilera, 2003; Castellano-Pozo *et al.*, 2013; Garcia-Pichardo *et al.*, 2017; Costantino and Koshland, 2018). Overexpression of *RNH1* did not affect the levels of R-loops at *CEN1* and *CEN3* in a WT strain or at the negative control region (179K) in WT

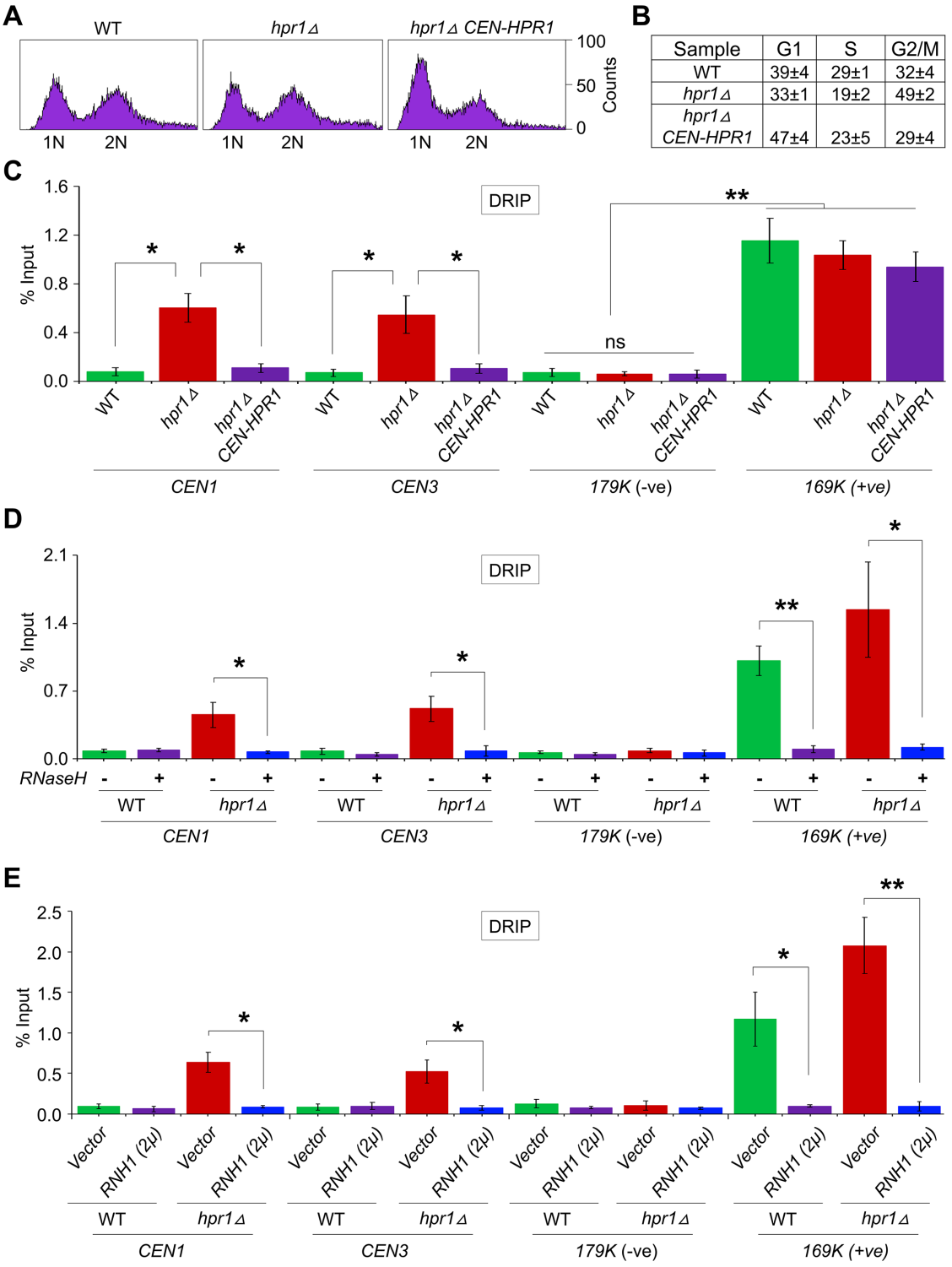

Sample	G1	S	G2/M
WT	39±4	29±1	32±4
hpr1Δ	33±1	19±2	49±2
hpr1Δ CEN-HPR1	47±4	23±5	29±4

FIGURE 2: Hpr1 prevents the accumulation of R-loops at the *CEN* chromatin. (A) FACS profile of logarithmically growing cultures of WT (YMB11246), *hpr1*Δ (YMB11247), and *hpr1*Δ *CEN-HPR1* (YMB11248) cells used for DRIP experiments. (B) Cell cycle categorization of strains from A representing the percentage of cells in G1, S, and G2/M. (C) Accumulation of R-loops at *CEN* chromatin in *hpr1*Δ and its suppression by *CEN-HPR1*. DRIP analysis of yeast strains from A using the S9.6 (anti–DNA-RNA hybrid) antibody. Levels of R-loops (% input) at *CEN*s (*CEN1* and *CEN3*), a negative control (179K), and a positive control (169K) were determined by DRIP-qPCR. Average from three biological replicates ± SE. ***p* value < 0.01, **p* value < 0.05, ns = statistically not significant, Student's *t* test. (D) Accumulation of R-loops at *CEN* chromatin in *hpr1*Δ cells with (+) or without (–) treatment with RNase H. DRIP analysis of WT (JG595) and *hpr1*Δ (YMB11097) using the S9.6 (anti–DNA-RNA hybrid) antibody. Levels of R-loops and statistical significance were determined as described in C. (E) Accumulation of R-loops at *CEN* chromatin in *hpr1*Δ cells with or without *RNH1* overexpression. DRIP analysis using the S9.6 (anti–DNA-RNA hybrid) antibody was performed for a WT strain with vector (YMB11210) or *2μ-RNH1* (YMB11211) and an *hpr1*Δ strain with vector (YMB11212) or *2μ-RNH1* (YMB11213). Levels of R-loops and statistical significance as described in C.

and *hpr1*Δ strains (Figure 2E). However, overexpression of *RNH1* significantly reduced the accumulation of R-loops at *CEN1* and *CEN3* in an *hpr1*Δ strain and at the positive control region (169K) in WT and *hpr1*Δ strains (Figure 2E). Taken together, these results show that Hpr1 prevents the accumulation of R-loops at *CEN*s.

CEN regions are enriched for ssDNA and R-loops during S-phase in an *hpr1*Δ strain

The enrichment of R-loops at *CEN*s in *hpr1*Δ cells prompted us to examine the consequence of *CEN* R-loops on cell cycle progression in *hpr1*Δ cells. Previous studies have shown that *hpr1*Δ strains are temperature sensitive at 37°C and exhibit synthetic growth defects when combined with mutants of the S-phase checkpoint (Gomez-Gonzalez *et al.*, 2009). WT and *hpr1*Δ cells were arrested in G1-phase and released at the permissive and restrictive temperatures, 30° and 37°C, respectively (Figure 3A). FACS analysis showed that while both WT and *hpr1*Δ cells progressed through S-phase similarly at 30°C, *hpr1*Δ cells showed a 10 to 15 min delay in the appearance of a mid–S-phase population at 37°C and never reached completion before the second S-phase initiated when compared to WT cells (Figure 3B). Next, we applied genome-wide mapping of ssDNA to monitor DNA replication dynamics (Feng *et al.*, 2006). The original design of the method used HU, an inhibitor of the ribonucleotide reductase, to slow down replication fork and enrich for ssDNA formation (Feng *et al.*, 2006). In the current experimental design, we instead used temperature sensitivity (37°C) to exert replication stress in cells synchronously entering S-phase in the absence of HU and sampled them throughout S-phase for ssDNA labeling (Figure 3A). By comparing ssDNA in *hpr1*Δ cells to WT cells, we asked if any specific regions of the chromosome experience replication fork delay and manifest in increased ssDNA formation after 10, 15, 20, and 25 min release from G1 arrest. We quantified the amount of ssDNA across the genome (all probes, Figure 3C) and within a 20 kb region centering on the *CEN* (Figure 3D). We did not observe a significant difference in enrichment of ssDNA across the genome between WT and *hpr1*Δ cells at all time points after release from G1 arrest (Figure 3C). However, specific enrichment of ssDNA at *CEN*s at both 15 and 20 min postrelease from G1 arrest, with statistically significant enrichment at 20 min, was observed in *hpr1*Δ cells (Figure 3D). Meta-analysis of ssDNA across a 4 kb region centering on all *CEN*s confirmed increased level of ssDNA in *hpr1*Δ cells at 20 min post–G1 release (Figure 3E). The enrichment levels of ssDNA at 20 min post–G1 release are shown along all of the 16 chromosomes for both WT and *hpr1*Δ strains (Figure 3F and Supplemental Figure S2). We next took a close-up view of ssDNA levels in a 4-kb window encompassing each of the 16 *CEN*s for 15 and 20 min post–G1 release. Our analysis uncovered 13 *CEN*s that showed higher levels of ssDNA in *hpr1*Δ than in the WT strain at 15 min post–G1 release (Supplemental Figure S3), and 12 such *CEN*s at 20 min post–G1 release (Supplemental Figure S4). Overall, we found enrichment of ssDNA at 15 *CEN*s (except *CEN10*) in *hpr1*Δ compared to the WT strain.

We hypothesized that R-loops at *CEN* chromatin contribute to the increased levels of *CEN*-associated ssDNA in *hpr1*Δ cells. The rationale for this is based on the fact that R-loop structure contains a displaced nontemplate ssDNA strand, opposite of the DNA:RNA hybrid on the template strand, and this ssDNA could serve as a template for labeling in our experiments. Hence, we performed DRIP using growth conditions as described above for ssDNA analysis. Experiments were done using WT and *hpr1*Δ strains arrested in G1-phase and at 20 min postrelease from G1 arrest at 37°C, referred to as S-phase in Figure 4 (FACS profiles are shown in Supplemental Figure S5). R-loops were not detected in G1- or S-phase cells at the negative control region (179K), but were enriched at the positive control region (169K) at both stages of the cell cycle, albeit higher in the S-phase cells in WT and *hpr1*Δ strains (Figure 4A). No significant enrichment of R-loops at *CEN* chromatin (*CEN1, CEN3, CEN6, CEN7*, and *CEN8*) was observed in G1- and S-phase in a WT strain. In agreement with a previous study that observed enrichment of R-loops at *CEN6* (Castellano-Pozo *et al.*, 2013), we observed higher levels of R-loops at *CEN6* and other *CEN*s (*CEN1, CEN3, CEN7*, and *CEN8*) in G1 cells of *hpr1*Δ strain when compared with WT strain. Higher levels of R-loops were observed at *CEN*s (*CEN1, CEN3, CEN6, CEN7*, and *CEN8*) in S-phase cells than in G1-phase cells of the *hpr1*Δ strain (Figure 4A), coincident with the enrichment of ssDNA in this strain at the same time point in the cell cycle (Figure 3, D and E). These results suggest that accumulation of *CEN* R-loops contributes to the enrichment of ssDNA in the *hpr1*Δ strain.

Recent studies have shown *CEN* lncRNA expression during S-phase of the cell cycle in a WT strain (Chen *et al.*, 2019; Ling and Yuen, 2019). We asked whether increased levels of *CEN* lncRNA contribute to enrichment of R-loops at *CEN*s. *CEN* lncRNA levels in G1- and S-phase cells of WT and *hpr1*Δ cells were examined by reverse transcription (RT)-qPCR. In agreement with previous reports (Chen *et al.*, 2019; Ling and Yuen, 2019), we found enrichment of *CEN* lncRNA (*CEN1, CEN3, CEN6, CEN7*, and *CEN8*) in S-phase cells of a WT strain. However, there was no significant difference in the levels of *CEN* lncRNA between WT and *hpr1*Δ strains (Figure 4B). Together, our results revealed that *CEN* R-loops in *hpr1*Δ contribute to the enrichment of ssDNA and that the accumulation of *CEN* R-loops is not solely dependent on the amount of *CEN* lncRNA transcription.

Accumulation of R-loops at *CEN* chromatin affects kinetochore integrity and biorientation

Our results for the interaction of Hpr1 with Cse4 and accumulation of R-loops at *CEN* in an *hpr1*Δ strain prompted us to examine the role of Hpr1 in the structural and functional integrity of the kinetochores. Hence, we performed chromatin IP (ChIP) experiments to determine the levels of Cse4 at the *CEN* chromatin in WT and *hpr1*Δ strains. FACS, microscopic examination of nuclear position, and cell morphology assays showed similar cell cycle profiles for WT and *hpr1*Δ strains used for these experiments (Figure 5A). *CEN*-associated Cse4 in the WT strain was significantly higher (~2.9% of input at *CEN1*, 3.0% at *CEN3*), whereas levels of *CEN*-associated Cse4 were significantly reduced in the *hpr1*Δ strain (~1.9% at *CEN1* and *CEN3*) (Figure 5B). No significant enrichment of Cse4 was detected at a negative control *ACT1* locus in either strain (Figure 5B).

The kinetochore protein Scm3 interacts with Cse4, both in vivo and in vitro, and Scm3 is required for association of Cse4 with *CEN* chromatin (Camahort *et al.*, 2007; Mizuguchi *et al.*, 2007; Stoler *et al.*, 2007). We reasoned that a defect in *CEN*-association of Scm3 might contribute to the reduced levels of Cse4 at the *CEN* in *hpr1*Δ strains. ChIP-qPCR revealed a significant reduction in enrichment of Scm3 at *CEN*s in the *hpr1*Δ strain (~30% reduction at *CEN1* and *CEN3*) when compared with the levels observed in a WT strain (Figure 5C). No significant enrichment of Scm3 was observed at a negative control *ACT1* locus (Figure 5C). Western blot analysis showed that the reduction in *CEN*-associated Cse4 and Scm3 observed in the *hpr1*Δ strain was not due to reduced expression of these proteins (Figure 5D). Previous studies have shown that Hpr1 plays a role in gene transcription and is preferentially required for the transcription of either GC-rich or long transcriptional units (Chavez and Aguilera, 1997; Chavez *et al.*, 2001). Hence, we examined if transcription of *CSE4*, *SCM3*, and other genes involved

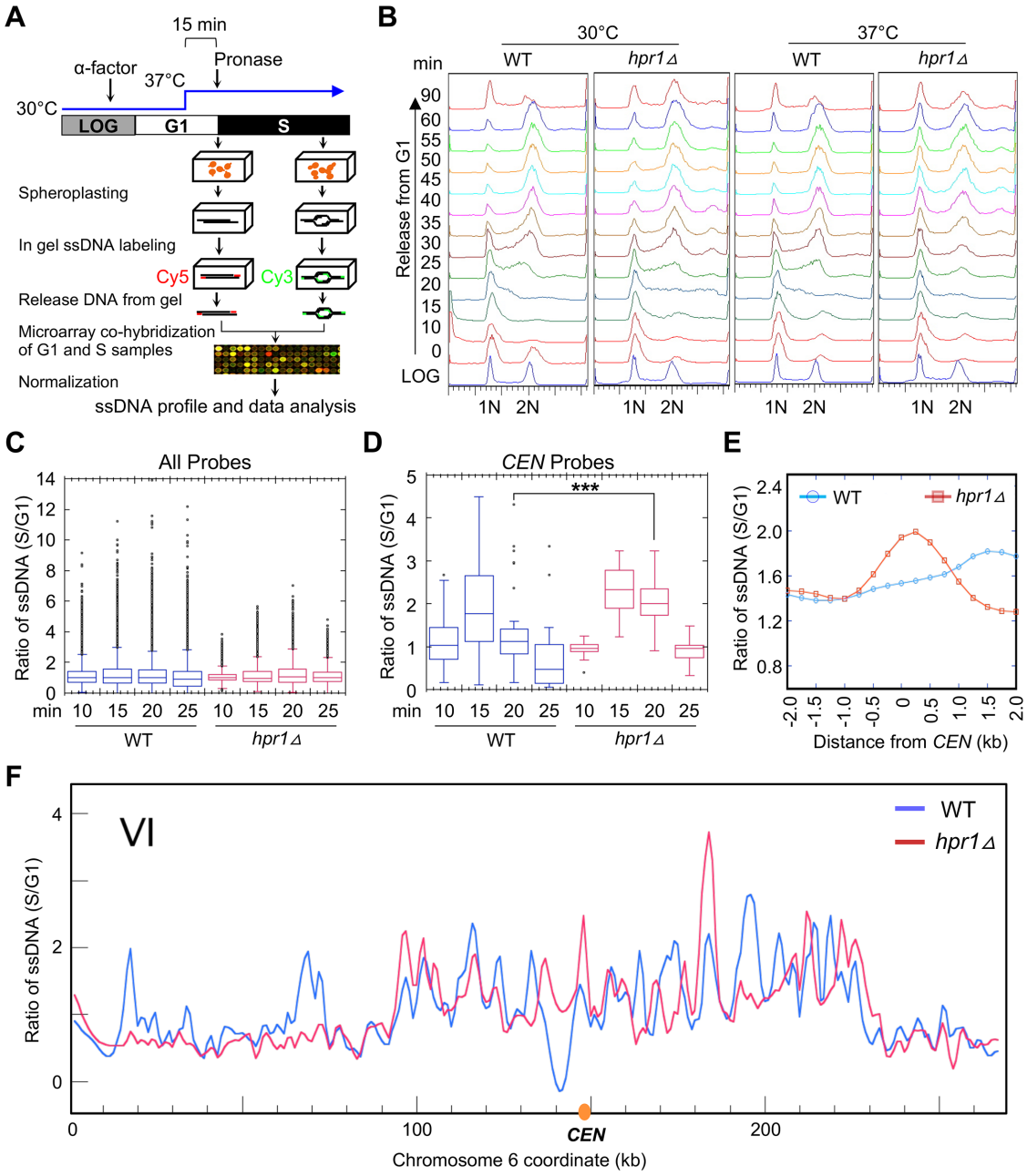

FIGURE 3: Genome-wide ssDNA mapping shows accumulation of ssDNA at *CEN*s in the *hpr1*Δ strain at the restrictive temperature (37°C). (A) Schematic presentation of genomic ssDNA mapping. Details of cell culture conditions, ssDNA labeling, and quantification are described in *Materials and Methods*. Briefly, cells synchronized in G1 by α-factor at 30°C were acclimatized to 37°C for 15 min before the release into S-phase by Pronase treatment. S-phase samples were collected every 5 min starting at 10 min postrelease, as shown in B. Select S-phase samples (10, 15, 20, and 25 min post–G1 release) were subject to ssDNA labeling, and each was cohybridized with a ssDNA labeled G1 control sample onto the microarray. (B) FACS profile of WT (BY4741) and *hpr1*Δ (BY4741 *hpr1*Δ) strains. Cells were collected as described in A. The positions of G1 and G2 cells are indicated by "1N" and "2N", respectively. (C, D) Box plots for quantification of ssDNA from cells sampled at the indicated time points post–release from G1- into S-phase for all probes on the microarray (C) and for probes overlapping only with the *CEN* (D). Statistical analysis was performed by analysis of variance followed by Tukey's multiple comparison. ***p value < 0.001. (E) Meta-analysis of ssDNA in a 4 kb window centering on the *CEN* for cells sampled at 20 min post–release from G1- into S-phase. (F) Example of a chromosomal plot of ssDNA on chromosome VI from cells sampled at 20 min at 37°C. For all chromosome plots, see Supplemental Figure S2.

in kinetochore assembly, protein modifications, DNA replication, and chromatin organization (Chavez *et al.*, 2001; Ciftci-Yilmaz *et al.*, 2018; Mishra *et al.*, 2018) was affected in the *hpr1*Δ strain. In agreement with previous studies (Chavez and Aguilera, 1997; Chavez *et al.*, 2001), we observed significant down-regulation of *ADR1* and *GAL83* and up-regulation of *SLD2* and *RRP12* in the *hpr1*Δ strain. However, no significant differences in transcription of *CSE4* or *SCM3* were observed between WT and *hpr1*Δ strains (Supplemental

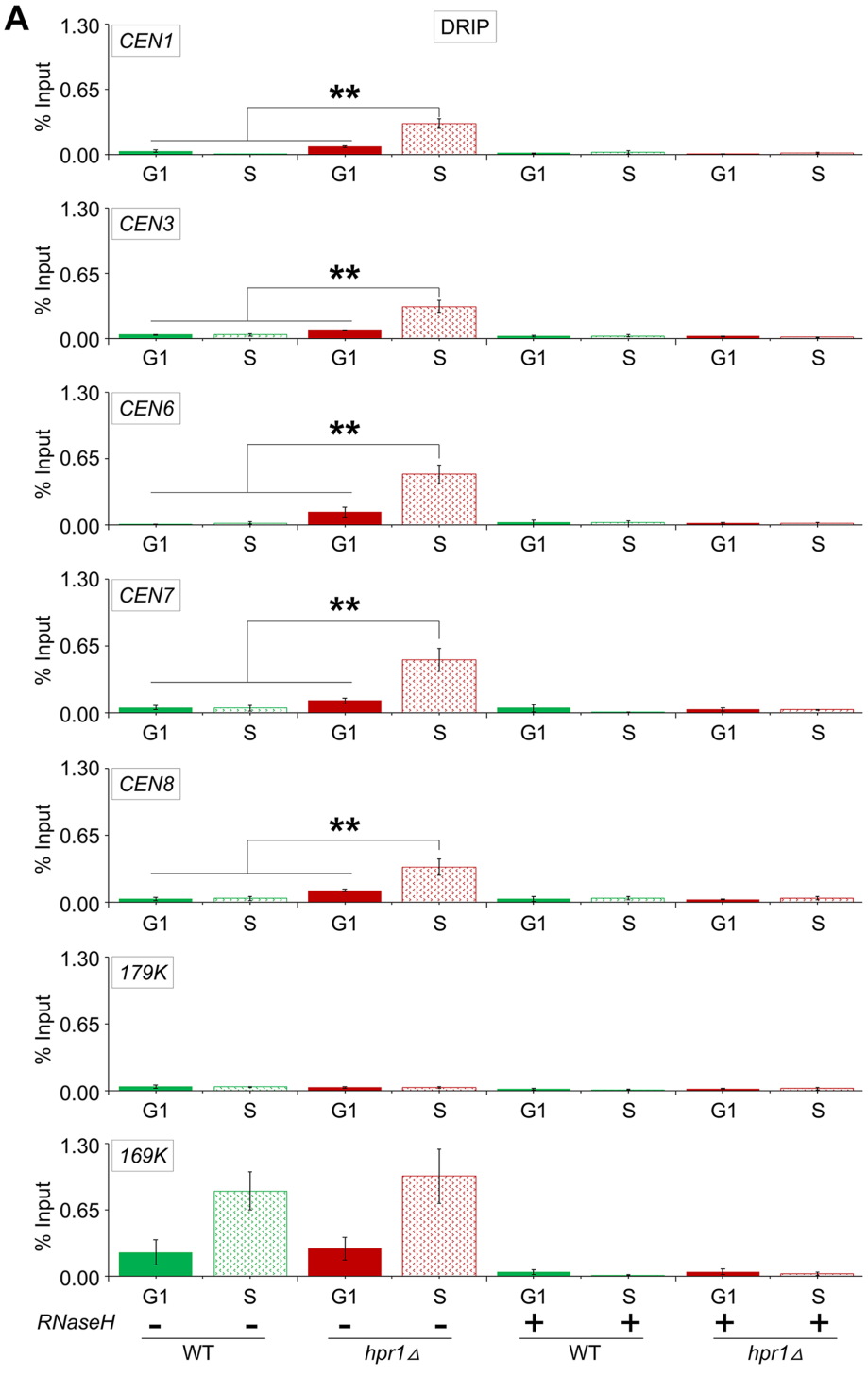

Figure S6). On the basis of these results, we conclude that reduced association of Cse4 and Scm3 to *CEN*s is not due to defects in transcription of *CSE4* or *SCM3* in *hpr1*Δ strain.

The reduced Cse4 at *CEN* prompted us to examine whether histone H3 replaces Cse4 at *CEN* chromatin in an *hpr1*Δ strain. Moreover, a previous study reported accumulation of H3S10P at *CEN*s upon deletion of *HPR1* (Castellano-Pozo *et al.*, 2013). ChIP-qPCR showed a similar enrichment of histone H3 at the *ACT1* locus in WT and *hpr1*Δ strains (~5% of input, Figure 5E). The enrichment of histone H3 at *CEN* chromatin in the *hpr1*Δ strain was about sixfold higher than in the WT strain (Figure 5E). However, the levels of histone H3 at *CEN* chromatin in the *hpr1*Δ strain were about 10- to 12-fold lower than those observed at the *ACT1* locus (Figure 5E).

Based on the reduced levels of Cse4 and Scm3 at *CEN* chromatin, we postulated that accumulation of R-loops at *CEN* chromatin would contribute to functional defects of the kinetochores in an *hpr1*Δ strain. Moreover, previous studies have shown that depletion of *CEN*-associated Scm3 leads to defects in sister kinetochore biorientation (Camahort *et al.*, 2007). Hence, we examined kinetochore biorientation in mitotic cells of WT and *hpr1*Δ strains by monitoring the localization of Ndc80-GFP (outer kinetochore protein that facilitates kinetochore–microtubule interactions) and Spc42-mCherry (protein that regulates the architecture of the spindle pole) expressed from their native promoters at the endogenous locus. In the WT strain, 81% of the cells had bioriented kinetochores, 7% mono-oriented, and 12%

FIGURE 4: Accumulation of R-loops contributes to the enrichment of ssDNA at the *CEN* chromatin. (A) Accumulation of R-loops at *CEN* coincides with the enrichment of *CEN*-derived ssDNA in an *hpr1*Δ strain. DRIP-qPCR analysis of WT (BY4741) and *hpr1*Δ (BY4741 *hpr1*Δ) strains was performed using the S9.6 (anti–DNA-RNA hybrid) antibodies. Average from three biological replicates ± SE. $^{**}p$ value < 0.01, Student's *t* test. (B) Expression of *CEN* lncRNA in S-phase is largely similar between WT and *hpr1*Δ strains. Total RNA was used in RT-qPCR to determine the expression level of *CEN* lncRNA (*CEN1, CEN3, CEN6, CEN7,* and *CEN8*) and *ACT1* lncRNA (control). Average from three biological replicates ± SE. ns = statistically not significant, Student's *t* test.

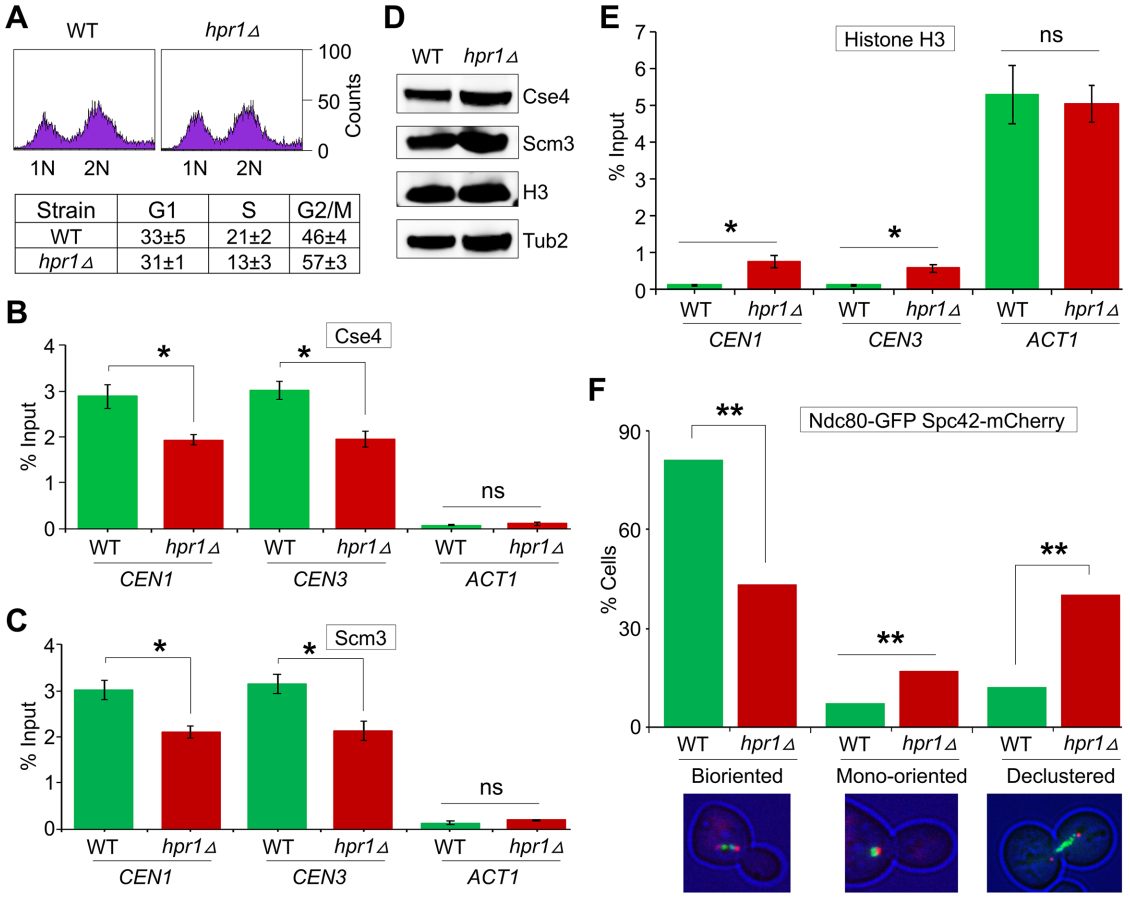

FIGURE 5: Accumulation of R-loops at *CEN* chromatin affects kinetochore integrity and biorientation. (A) FACS profile and cell cycle categorization of logarithmically growing cultures of WT (JG595) and *hpr1*Δ (YMB11097) strains. (B) *CEN*-associated Cse4 is reduced in an *hpr1*Δ strain. ChIP for Cse4 was performed using anti-Myc agarose beads (A7470; Sigma Aldrich). Cse4 enrichment at *CEN1*, *CEN3*, and a negative control (*ACT1*) was determined by qPCR and is presented as % input. Average from three biological replicates ± SE. *p value < 0.05, ns = statistically not significant, Student's t test. (C) *CEN*-associated Scm3 is reduced in an *hpr1*Δ strain. ChIP for Scm3 was performed using anti-Flag agarose beads (A2220; Sigma Aldrich). Scm3 enrichment at *CEN1*, *CEN3*, and a negative control (*ACT1*) was determined by qPCR and is presented as % input. Average from three biological replicates ± SE. *p value < 0.05, ns = statistically not significant, Student's t test. (D) Protein levels of Cse4 and Scm3 are not reduced in an *hpr1*Δ strain. Western blotting was done using the whole cell extracts from strains described in A. (E) Histone H3 associates with *CEN* chromatin in the *hpr1*Δ strain. ChIP for histone H3 was done using anti-H3 antibodies (Cat# ab176842; Abcam). Histone H3 enrichment at *CEN1*, *CEN3*, and *ACT1* was determined by qPCR and is presented as % input. Average from three biological replicates ± SE. *p value < 0.05, ns = statistically not significant, Student's t test. (F) Deletion of *HPR1* causes defects in kinetochore biorientation. WT (KBY6380) and *hpr1*Δ (KBY6432) strains containing Ndc80-GFP and Spc42-mCherry were grown at room temperature (25°C). The cutoff for metaphase spindle length was 1.7 μm. Spc42-mCherry was used as a spindle pole marker. Representative images showing the position of Ndc80-GFP (green) and Spc42-mCherry (red) are shown. Percentage of cells showing bioriented, mono-oriented (large budded cell with unseparated SPBs), and declustered kinetochores are shown (n = 181 cells). Statistical significance was determined by χ^2 test. **p value < 0.01.

declustered kinetochores whereas, in the *hpr1*Δ strain, 43% of the cells had bioriented kinetochores, 17% mono-oriented, and 40% declustered kinetochores (Figure 5F). The defect in kinetochore biorientation in the *hpr1*Δ strain was about threefold higher than in the WT strain (Figure 5F), similar to that reported for mutants defective in kinetochore structure and function, such as Dam1, Mcm21, Stu2, and Spc29 (Cheeseman *et al.*, 2002; Yoder *et al.*, 2005; Ng *et al.*, 2009; Miller *et al.*, 2019). Kinetochore declustering is diagnostic of weakened or altered kinetochores, due to the inability to maintain microtubule attachment during dynamic cycles of microtubule growth or shortening, or defective interactions between adjacent kinetochores that contribute to their spatial clustering. The results showing defects in kinetochore biorientation in the *hpr1*Δ strain together with the reduced levels of *CEN*-associated Cse4 and Scm3 suggest that the accumulation of R-loops at *CEN* chromatin affects the structural and functional integrity of kinetochores.

Accumulation of R-loops at *CEN* contributes to CIN

Our results for accumulation of R-loops at *CEN*, reduced levels of *CEN*-associated Cse4 and Scm3, and defects in kinetochore biorientation in the *hpr1*Δ strain led us to examine whether these strains exhibit a CIN phenotype. We first examined the growth phenotype of WT and *hpr1*Δ strains exposed to benomyl. Benomyl treatment causes depolymerization of mitotic spindles, and benomyl sensitivity

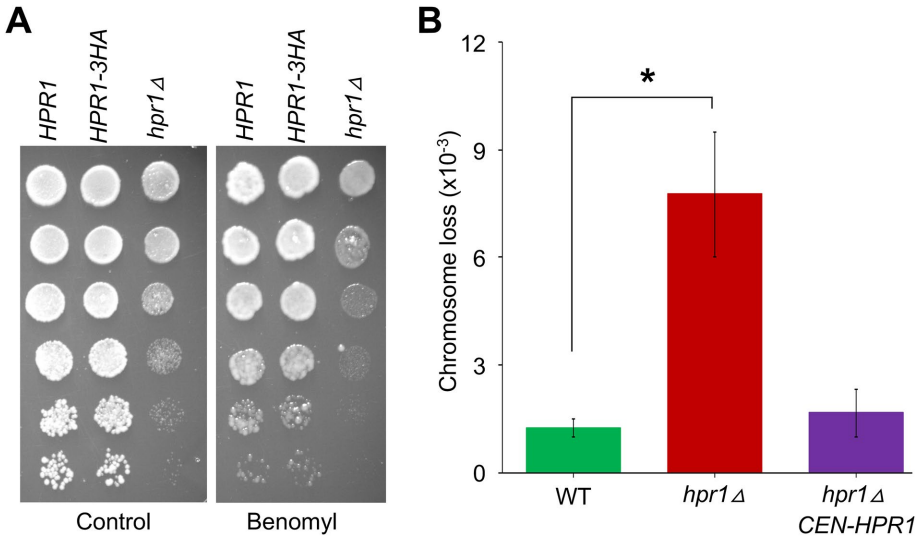

FIGURE 6: Accumulation of R-loops at *CEN* chromatin contributes to CIN. (A) An *hpr1*Δ strain displays sensitivity to benomyl. Serial (fivefold) dilutions of *HPR1* (JG595), *HPR1-3HA* (YMB11085), and *hpr1*Δ (YMB11097) strains were plated on YPD plates with or without benomyl (10 µg/ml) and grown for 3 d at 25°C. (B) Errors in chromosome segregation are increased in *hpr1*Δ strain. Frequency of CF loss in WT (YPH1018), *hpr1*Δ (YMB11087), and *hpr1*Δ *CEN-HPR1* (YMB11251) strains were measured by a colony color assay as detailed in *Materials and Methods*. Average from three biological experiments ± SE. **p* value < 0.05, Student's *t* test.

is a feature commonly observed in mutants with defects in chromosome segregation (Spencer *et al.*, 1990; Hyland *et al.*, 1999). Our results showed that *hpr1*Δ strains exhibit increased sensitivity to benomyl when compared to a WT and *HPR1-3HA* strain (Figure 6A). Notably, a previous study has observed increased frequency of loss for chromosoms V and XV in a homozygous diploid *hpr1*Δ strain using fluctuation analysis on populations of cells (Santos-Rosa and Aguilera, 1994). To examine the chromosome transmission fidelity, we constructed a haploid *hpr1*Δ strain carrying a reporter chromosome fragment (CF) and determined the frequency of CF loss using a highly sensitive, visible colony color assay that is based on plating of individual cells (Spencer *et al.*, 1990). The frequency of CF loss in *hpr1*Δ strains is about sixfold higher than in the WT strain (Figure 6B), which is similar to the CF loss in kinetochore mutants, such as *ndc10-1* and *mad1*Δ strains (Kastenmayer *et al.*, 2005; Ma *et al.*, 2012). The CF loss phenotype of *hpr1*Δ strain is complemented by a plasmid-based *HPR1* expressed from its native promoter (Figure 6B). On the basis of these results, we conclude that accumulation of R-loops at *CEN* chromatin contributes to CIN.

Overexpression of *RNH1* suppresses CIN and kinetochore biorientation defects in an *hpr1*Δ strain

To further confirm that accumulation of R-loops at *CEN* chromatin contributes to CIN and defects in kinetochore biorientation in *hpr1*Δ strains, we examined whether these phenotypes would be suppressed upon overexpression of *RNH1*. We assayed CIN in WT and *hpr1*Δ strains overexpressing *RNH1*. As noted previously (Figure 6B), we observed a significantly higher frequency of CF loss in *hpr1*Δ with vector than in the WT with vector (Figure 7A). The frequency of CF loss in the *hpr1*Δ strain was significantly suppressed by overexpression of *RNH1* when compared to the *hpr1*Δ strain containing vector alone (Figure 7A). The CF loss phenotype was largely similar between WT and *hpr1*Δ strains overexpressing *RNH1*, although overexpression of *RNH1* in the WT strain showed slightly higher CF loss than the WT with vector alone (Figure 7A).

We next examined the effect of *RNH1* overexpression on kinetochore biorientation and kinetochore clustering in WT and *hpr1*Δ strains. The *hpr1*Δ strain with vector showed significant defects in kinetochore biorientation when compared to the WT strain with vector alone (Figure 7B). Overexpression of *RNH1* suppressed kinetochore biorientation defects in the *hpr1*Δ strain with no significant effect in the WT strain (Figure 7B). Kinetochores in budding yeast form a single cluster close to the spindle pole bodies (SPB) from G1- through late S-phase where all 16 *CEN*s are clustered (Jin *et al.*, 1998, 2000; Joglekar *et al.*, 2008). Hence, we examined the phenotype of kinetochore clustering in G1 cells of the WT or *hpr1*Δ overexpressing *RNH1* (Figure 7C). In the WT strain with vector alone about 20% of cells had declustered or detached kinetochores and this was not affected by overexpression of *RNH1* (Figure 7D), whereas, in *hpr1*Δ with vector alone, 89% of the cells had declustered kinetochores, and this defect was suppressed by overexpressing *RNH1* (Figure 7D). Remarkably, there was about 40% suppression in defects in kinetochore clustering in the *hpr1*Δ strain overexpressing *RNH1* (Figure 7D). Taken together, these results show that accumulation of R-loops at *CEN* contributes to CIN phenotype and *RNH1* overexpression suppresses CIN, kinetochore biorientation, and kinetochore clustering defects in *hpr1*Δ strains.

DISCUSSION

R-loops are not detected at *CEN*s in a WT budding yeast strain (Costantino and Koshland, 2018), and the physiological consequences due to accumulation of R-loops at *CEN* chromatin have not been investigated. We examined the effect of R-loops in kinetochore function and chromosome segregation using deletion of *HPR1*, which causes accumulation of R-loops at *CEN* chromatin (Huertas and Aguilera, 2003). We herein report that accumulation of R-loops at *CEN*s contributes to defects in kinetochore integrity and CIN. Our results show an in vivo interaction of Hpr1 with Cse4 and accumulation of R-loops and ssDNA at *CEN*s in *hpr1*Δ strains. Accumulation of R-loops at *CEN* chromatin contributes to reduced levels of Cse4 and Scm3, with a concomitant increase in histone H3 at *CEN*s. Defects in kinetochore biorientation and CIN phenotype in *hpr1*Δ strains are suppressed by overexpression of *RNH1*. Our studies provide mechanistic insights into how accumulation of R-loops at *CEN* contributes to defects in kinetochore integrity and CIN.

Our results from three independent in vivo experiments showed accumulation of R-loops at *CEN* chromatin in *hpr1*Δ strains. Treatment with RNase H, overexpression of *RNH1*, and transformation with a plasmid containing WT *HPR1* reduced the accumulation of R-loops at *CEN*s in *hpr1*Δ strains. Notably, treatment with RNase H and overexpression of *RNH1*, both of which specifically degrade RNA engaged in R-loops, have been used to validate the presence of R-loops (Huertas and Aguilera, 2003; Castellano-Pozo *et al.*, 2013; Garcia-Pichardo *et al.*, 2017; Costantino and Koshland, 2018; Allison and Wang, 2019). Although transcription is a prerequisite for R-loop formation (Allison and Wang, 2019; Rondon and Aguilera, 2019), our data show that increased transcription of *CEN* lncRNA alone is not

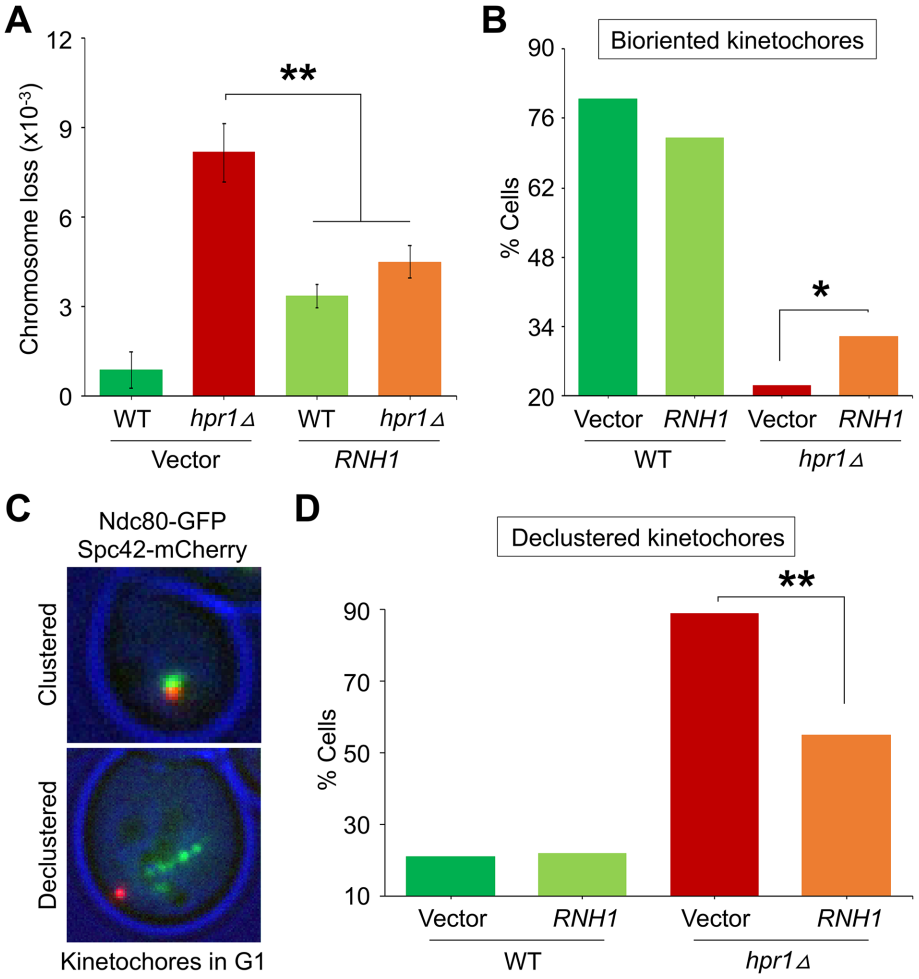

FIGURE 7: Overexpression of *RNH1* suppresses CIN, kinetochore biorientation, and kinetochore clustering defects in *hpr1*Δ strains. (A) *RNH1* overexpression suppresses the frequency of chromosome segregation errors in the *hpr1*Δ strain. Frequencies of CF loss in WT with vector (YMB11206) or *2μ-RNH1* (YMB11207) and *hpr1*Δ with vector (YMB11208) or *2μ-RNH1* (YMB11209) strains were measured by a colony color assay as detailed in *Materials and Methods*. Average from three biological experiments ± SE. ***p* value < 0.01, Student's *t* test. (B) *RNH1* overexpression suppresses kinetochore biorientation defects in metaphase cells of *hpr1*Δ strains. WT with vector (YMB11494; $n = 135$ cells) or *2μ-RNH1* (YMB11495; $n = 123$ cells) and *hpr1*Δ with vector (YMB11496; $n = 134$ cells) or *2μ-RNH1* (YMB11497; $n = 216$ cells) strains containing Ndc80-GFP and Spc42-mCherry were grown at room temperature (25°C). The cutoff for metaphase spindle length was 1.7 μm. Spc42-mCherry was used as a spindle pole marker. Percentages of cells showing bioriented kinetochores are shown. Statistical significance was determined by χ^2 test. **p* value < 0.05. (C) Representative images of G1 cells depicting clustered and declustered kinetochores based on the position of Ndc80-GFP (green) and Spc42-mCherry (red). (D) *RNH1* overexpression suppresses kinetochore clustering defects of *hpr1*Δ cells in G1. WT with vector (YMB11494; $n = 104$ cells) or *2μ-RNH1* (YMB11495; $n = 103$ cells) and *hpr1*Δ with vector (YMB11496; $n = 100$ cells) or *2μ-RNH1* (YMB11497; $n = 292$ cells) carrying Ndc80-GFP and Spc42-mCherry were grown at room temperature (25°C) to LOG phase, and G1 cells were selected based on the cell morphology (single-celled, no bud). Percentage of cells showing declustered kinetochores in G1 are shown. Statistical significance was determined by χ^2 test. ***p* value < 0.01.

these observations, we propose that small amounts of RNA are sufficient for the seeding and/or initiation of R-loops at *CEN*s, and once established, Hpr1 and the underlying chromatin environment determine the fate and stability of R-loops. We detected significant enrichment of ssDNA at *CEN* chromatin in *hpr1*Δ cells. We posit that the *CEN*-associated ssDNA in *hpr1*Δ cells is the result of R-loop formation because we have detected R-loops at *CEN* chromatin in these strains.

We observed reduced levels of *CEN*-specific histone H3 variant Cse4 and its assembly factor Scm3 with a concomitant increase in histone H3 at *CEN* chromatin, defects in kinetochore biorientation, and clustering resulting in CIN in *hpr1*Δ strains. We have previously reported that overexpression of histone H3 contributes to reduced levels of Cse4 at *CEN* chromatin, increased chromosome loss in WT strains, and synthetic dosage lethality in kinetochore mutants (Au *et al.*, 2008). Our results for increased association of histone H3 at *CEN* chromatin in *hpr1*Δ strains are consistent with previous studies showing a link between R-loops and enrichment of H3S10P, a mark for chromatin condensation, at *CEN6* in *hpr1*Δ G1 cells (Castellano-Pozo *et al.*, 2013). Notably, the recruitment of Cse4 to kinetochores occurs during a brief window in early S-phase (~10 min post–bud emergence) of the cell cycle, and once recruited, it remains stably associated with kinetochores throughout the cell cycle (Pearson *et al.*, 2004). Depletion of Cse4 during S-phase causes phenotypes reminiscent of a defective kinetochore that are manifested in cells undergoing mitosis (Stoler *et al.*, 1995; Collins *et al.*, 2005). Furthermore, defects in kinetochore structure in mutants corresponding to Dam1, Mcm21, Stu2, and Spc29 lead to defects in kinetochore biorientation (Cheeseman *et al.*, 2002; Yoder *et al.*, 2005; Ng *et al.*, 2009; Miller *et al.*, 2019) such as those that we observed in *hpr1*Δ strains. We propose that the presence of histone H3 and R-loops at *CEN* chromatin in G1 cells creates a chromatin environment that is not conducive for the Scm3-mediated recruitment of Cse4 in early S-phase, and that the reduced levels of *CEN*-associated Cse4 and other proteins contribute to mitotic defects in *hpr1*Δ cells. Our results for the in vivo interaction of Hpr1 with Cse4 and other experimental evidence support this hypothesis. For example, we have shown that *hpr1*Δ strains exhibit 1) reduced levels of Cse4 and Scm3 and increased levels of histone H3 at *CEN* chromatin, 2) defects in kinetochore biorientation and kinetochore clustering, and 3) the CIN phenotype.

sufficient for accumulation of R-loops at *CEN* chromatin. For example, WT cells arrested in S-phase show higher levels of *CEN* lncRNA than cells arrested in G1-phase; however, R-loops were not detected at *CEN* chromatin in either of these cells. Furthermore, even though the levels of *CEN* lncRNA are similar in WT and *hpr1*Δ strains arrested in S-phase, significantly higher enrichment of R-loops at *CEN* chromatin was observed in *hpr1*Δ S-phase cells. On the basis of

Overexpression of *RNH1* suppressed defects in kinetochore biorientation, kinetochore clustering, and CIN in *hpr1*Δ strains even

though they were not restored to levels observed in the WT strain with vector alone. Furthermore, we observed higher chromosome loss due to overexpression of *RNH1* in WT strains. Since *RNH1* overexpression does not specifically remove R-loops at *CEN* chromatin alone, we propose that a threshold of R-loops throughout the genome is needed for faithful chromosome segregation and that accumulation of R-loops at *CEN* chromatin affects kinetochore function. The defects in kinetochore biorientation and kinetochore clustering observed at a single-cell level provide the strongest evidence for how accumulation of R-loops at *CEN* chromatin contributes to defects in the integrity of the kinetochore, leading to defects in mitosis in *hpr1*Δ strains.

Our results from budding yeast have begun to provide mechanistic insights into how accumulation of R-loops at *CEN* chromatin perturbs kinetochore integrity and contributes to CIN. In maize, R-loops at *CEN*s correlate with lower levels of C-loops and reduced localization of CENH3 (Cse4 homolog) to centromeres (Liu *et al.*, 2020); however, the physiological consequences of R-loops have not been defined. In human cells, R-loops in S-phase interfere with DNA replication, resulting in genomic instability, whereas R-loops in mitosis activate the mitosis-specific ATR checkpoint pathway to prevent errors in chromosome segregation (Kabeche *et al.*, 2018). Notably, ATR associates with human *CEN*s in mitosis mediated by Aurora-A and CENP-F (centromere protein F) (Kabeche *et al.*, 2018). ATR activity at mitotic *CEN*s facilitates the recruitment of replication protein A–coated *CEN* R-loops, leading to the stimulation of Aurora-B kinase, which in turn prevents the formation of lagging chromosomes (Kabeche *et al.*, 2018). Our results show increased chromosome loss due to accumulation of *CEN* R-loops in the *hpr1*Δ strain. The core-*CEN* in budding yeast is small in size (~125 base pairs) and occupied by a single Cse4 nucleosome (Furuyama and Biggins, 2007; Bloom and Costanzo, 2017), whereas human *CEN*s are megabases in size and contain multiple CENP-A nucleosomes interspersed with canonical histone H3 nucleosomes (McKinley and Cheeseman, 2016; Andronov *et al.*, 2019). Furthermore, there are multiple kinetochore–microtubule (KT-MT) attachments in higher eukaryotes for each *CEN* as opposed to a single KT-MT attachment for each *CEN* in budding yeast (Furuyama and Biggins, 2007; McKinley and Cheeseman, 2016; Bloom and Costanzo, 2017; Andronov *et al.*, 2019). The presence of R-loops at complex *CEN* chromatin in mitosis may provide an additional surveillance mechanism to monitor multiple KT-MT attachments for faithful chromosome segregation in human cells.

We propose a model in which accumulation of R-loops at *CEN* chromatin contributes to defects in kinetochore integrity and promotes CIN (Figure 8). Consistent with this model, we observed that *RNH1* overexpression, which degrades the RNA moiety of R-loops, suppressed CIN, kinetochore biorientation, and kinetochore clustering defects in *hpr1*Δ strains. Taken together, we conclude that R-loops and increased levels of histone H3 at the *CEN* chromatin interfere with the assembly and function of the kinetochore. On the microtubule side of the kinetochore, it has long been appreciated that kinetochores are able to maintain constant interaction with microtubule plus ends that are constantly switching states from growth to shortening. On the DNA side of the kinetochore, we are starting to appreciate the involvement of active transcription. There is an optimal level of RNA transcription required for centromere/kinetochore function, and levels above or below lead to failures in segregation (Hill and Bloom, 1987; Ohkuni and Kitagawa, 2012). The accumulation of R-loops and H3 at *CEN*s may be one of the key mechanisms of *CEN* dysfunction. This may act as a physical barrier and interfere with the structural configuration and geometric oscillation of kinetochores required for the localization of kinetochore proteins and chromosome stability. Future studies should help us understand how Hpr1 prevents accumulation of R-loops and the implications of R-loops in geometric oscillation of kinetochores during the cell cycle and chromosome segregation. Moreover, R-loops have been implicated in a number of human

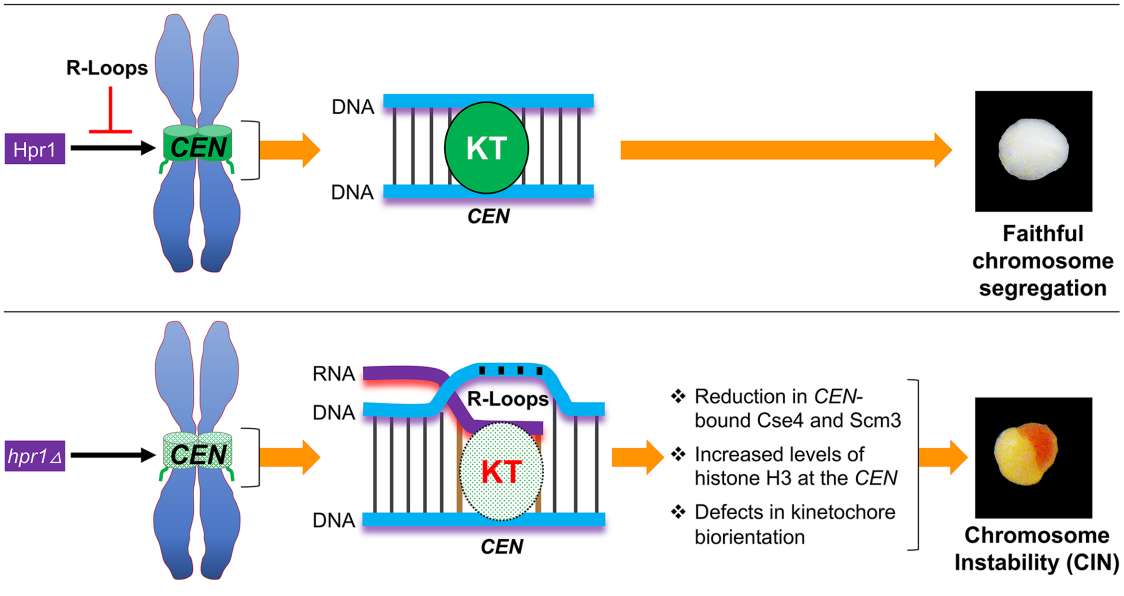

FIGURE 8: Schematic model proposing that accumulation of R-loops at *CEN* chromatin contributes to CIN. In a WT strain, the presence of Hpr1 prevents the accumulation of R-loops at *CEN* chromatin leading to faithful chromosome segregation and white colonies due to retention of the reporter CF. In an *hpr1*Δ strain, R-loops accumulate at the *CEN* chromatin and this contributes to reduced levels of Cse4 and Scm3, increased levels of histone H3 at *CEN* chromatin, defects in kinetochore biorientation, benomyl sensitivity, and CIN as depicted by half red/half white colonies due to loss of reporter CF.

diseases, including cancers (Groh and Gromak, 2014; Wells *et al.*, 2019). Hence, it will be of interest to examine the physiological consequences of R-loops at *CEN* chromatin in other systems including human cancers.

MATERIALS AND METHODS

Yeast strains, plasmids, and growth conditions

Budding yeast strains, plasmid constructs, and PCR primers used in this study are listed in Table 1. Strains were grown in yeast peptone dextrose medium (1% yeast extract, 2% Bacto-peptone, 2% glucose; YPD) or in synthetic medium with supplements to allow for the selection of plasmids.

IP and Western blotting

Extracts were prepared from yeast cells grown to logarithmic phase at 30°C in YPD medium. IP experiments were done with anti-HA (A2095; Sigma Aldrich) and anti-Myc (A7470; Sigma Aldrich) agarose antibodies following the procedure as described (Mishra *et al.*, 2011, 2018). Total proteins were extracted with the trichloroacetic acid (TCA) procedure (Kastenmayer *et al.*, 2005) and quantified using the Bio-Rad DC protein quantitation assay (Bio-Rad Laboratories, Hercules, CA). Protein samples for Western blotting were size separated on SDS–polyacrylamide gels and transferred to a 0.45-µm nitrocellulose membrane. Primary antibodies used were anti-Myc (a-14, sc-789; Santa Cruz Biotechnology), anti-HA (H6908; Sigma Aldrich), and anti-Tub2 (Au *et al.*, 2008; Mishra *et al.*, 2016). Secondary antibodies were horseradish peroxidase (HRP)-conjugated sheep anti-mouse immunoglobulin G (IgG) (NA931V) and HRP-conjugated sheep anti-rabbit IgG (NA934V), both obtained from Amersham Biosciences.

ChIP and qPCR

ChIP experiments were performed with three independent biological replicates using the approach as described previously (Mishra *et al.*, 2007, 2011). Antibodies used to capture DNA-protein complexes were anti-HA agarose (A2095; Sigma Aldrich), anti-Myc agarose (A7470; Sigma Aldrich), anti-Flag agarose (A2220; Sigma Aldrich), and anti-histone H3 (ab176842; Abcam). ChIP-qPCR was done using Fast SYBR Green Master Mix in 7500 Fast Real Time PCR System (Applied Biosystems, Foster City, CA) following conditions described previously (Mishra *et al.*, 2015). The enrichment as presented as percent input was determined using the $_{\Delta\Delta}C_T$ method (Livak and Schmittgen, 2001).

Flow cytometry and cell morphology analysis

For FACS analysis, cells were fixed in fixation buffer (70% ethanol, 0.2 M Tris, pH 7.4), washed twice in 0.2 M Tris-buffer (pH 7.4), and then treated with RNase A (0.2 M Tris-buffer [pH 7.4]; 0.1 mg/ml RNase A) at 37°C for 3 h followed by proteinase K treatment (final concentration of 0.2 mg/ml) at 50°C for 1 h. Cells were washed twice in 0.2 M Tris-buffer (pH 7.4) and stained with propidium iodide solution (0.2 M Tris-buffer [pH 7.4], 15 µg/ml propidium iodide) overnight at 4°C. Sample were processed using a FACS Calibur flow cytometer and analyzed using Cell Quest Pro software (BD Biosciences). Cells were examined under the microscope (Axioskop 2; Zeiss), and cell cycle stages were determined based on nuclear position and cell morphology as described previously (Mishra *et al.*, 2011).

DRIP-qPCR experiments

DRIP experiments were performed as described previously (Castellano-Pozo *et al.*, 2013; Costantino and Koshland, 2018; Kabeche *et al.*, 2018) with some minor modifications. Briefly, cells were dissolved in spheroplasting buffer (20 mM HEPES, pH 7.4, 1.2 M sorbitol, 0.5 mM phenylmethylsulfonyl fluoride [PMSF]), containing Zymolyase 100T (0.04 mg/ml; MP Biomedicals) and β-mercaptoethanol (5 µl/ml; Sigma Aldrich), and incubated at 30°C for spheroplast preparation. Spheroplasting was monitored by OD_{800} measurements in 1% SDS, and reactions were stopped when >90% spheroplasting was achieved by washing in postspheroplasting buffer (20 mM PIPES, pH 6.8, 1.2 M sorbitol, 1 mM $MgCl_2$, 1 mM PMSF). DNA extractions were done using the QIAamp DNA Blood Mini Kit (Cat# 51104; Qiagen). Spheroplasts were resuspended in lysis buffer AL and sonicated to obtain an average fragment size of ~500 base pairs. DNA was extracted from sonicated spheroplasts using Qiagen columns following manufacturer's recommendations (Cat# 51104; Qiagen), and eluted in nuclease-free AE buffer. DNA was treated with RNase H (Cat# M0297S; New England Biolabs) before DRIP experiments as described previously (El Hage *et al.*, 2010). Control (untreated) and RNase H–treated DNA was dissolved in 1× FA buffer (50 mM HEPES-Na, pH 7.6, 150 mM NaCl, 1 mM EDTA, 1% Triton X-100, 0.1% sodium deoxycholate, and 1× protease inhibitor cocktail [Sigma]), and DRIP was performed by adding 5 µg of S9.6 antibodies (Kera Fast) conjugated to magnetic Protein-A Dynabeads (Invitrogen) and incubating overnight at 4°C. Beads were then washed at room temperature for 5 min with 1× FA buffer (three times), 1× FA with 500 mM NaCl (once), RIPA (250 mM LiCl, 0.5% NP-40, 0.5% sodium deoxycholate, 1 mM EDTA, and 10 mM Tris-HCl) buffer (once), and finally twice with 1× TE buffer. DNA was then eluted from the beads with 100 µl of elution buffer (0.5% SDS, 10 mM EDTA, 25 mM Tris-HCl, pH 7.6), treated with proteinase K, and purified using MinElute columns (Cat# 28004; Qiagen). The percentage of the hybrid signal was quantified using qPCR on DNA from IP and total input with the Fast SYBR-Green Master Mix (Applied Biosystems) using PCR primers from *CEN*s (*CEN*1, *CEN3*, *CEN6*, *CEN7*, and *CEN8*) and control regions: R-loop–positive region (169K), and R-loop–negative region (179K), for which primers were designed based on a previous study (Costantino and Koshland, 2018). The amplification conditions were initial denaturation at 95°C for 20 s followed by cycling of 95°C for 3 s and 60°C for 30 s (data acquisition step) in a 7500 Fast-Real Time PCR System (Applied Biosystems). Three independent biological replicates were performed for each sample, and data are presented as percent input calculated using the $_{\Delta\Delta}C_T$ method (Livak and Schmittgen, 2001).

Genome-wide microarray-based analysis of ssDNA

Cells grown exponentially at 30°C were synchronized in G1 by addition of 3 µM α-factor. Fifteen minutes before the release from G1- into S-phase by addition of 0.3 mg/ml Pronase, half of the cells were shifted to 37°C and used for ssDNA mapping. As control (for FACS analysis), the other half of the culture was maintained at 30°C and released into S-phase at 30°C. Following the release from G1- into S-phase, cells were sampled at 10, 15, 20, and 25 min and subjected to ssDNA labeling. A G1 control sample was collected before Pronase addition and also labeled for ssDNA. Each S-phase sample was paired with the G1 control, differentially labeled with Cy3- and Cy5-dUTP, respectively, and cohybridized onto the same microarray slide (Agilent 4 × 44 k ChIP-to-chip microarray). ssDNA labeling and quantification were performed as previously described (Feng *et al.*, 2006). The genome-wide data are available from the National Center for Biotechnology Information (NCBI) GEO repository under the accession reference number GSE151849.

RNA extraction and RT-qPCR

Total RNA was extracted from the yeast cells using the Qiagen RNeasy kit and subjected to rigorous DNase treatment according

Saccharomyces cerevisiae		
Strain	**Genotype**	**Reference**
BY4741	*MATa ura3Δ0 leu2Δ0 his3Δ1 met15Δ0*	Open Biosystems
BY4741 hpr1Δ	*MATa ura3Δ0 leu2Δ0 his3Δ1 met15Δ0 hpr1Δ:KAN*	Open Biosystems
YPH1018	*MATα ura3-52 lys2-801 ade2-101 trp1Δ63 his3Δ200 leu2Δ1 CFIII (CEN3L.YPH278) HIS3 SUP11*	Phil Hieter, University of British Columbia, Vancouver, BC, Canada
JG595	*MATa ura3-1 leu2,3-112 his3-1 trp1-1 ade2-1 can1-100 Δbar1 CSE4-12Myc::URA3 SCM3-3Flag::KANMX*	Camahort *et al.*, 2007
YMB11085	*MATa ura3-1 leu2,3-112 his3-1 trp1-1 ade2-1 can1-100 Δbar1 CSE4-12Myc::URA3 SCM3-3Flag::KANMX HPR1-3HA::HIS3*	This study
YMB11087	*MATα ura3-52 lys2-801 ade2-101 trp1Δ63 his3-Δ200 leu2Δ1 hpr1Δ::TRP1 CFIII (CEN3L.YPH278) HIS3 SUP11*	This study
YMB11097	*MATa ura3-1 leu2,3-112 his3-1 trp1-1 ade2-1 can1-100 Δbar1 CSE4-12Myc::URA3 SCM3-3Flag::KANMX hpr1Δ::TRP1*	This study
YMB11210	*MATα ura3-52 lys2-801 ade2-101 trp1Δ63 his3Δ200 leu2Δ1 URA3-Vector (pRS426)*	This study
YMB11211	*MATα ura3-52 lys2-801 ade2-101 trp1Δ63 his3Δ200 leu2Δ1 pGPD-RNH1-HA::URA3 (pBB39)*	This study
YMB11212	*MATα ura3-52 lys2-801 ade2-101 trp1Δ63 his3Δ200 leu2Δ1 hpr1Δ::TRP1 URA3-Vector (pRS426)*	This study
YMB11213	*MATα ura3-52 lys2-801 ade2-101 trp1Δ63 his3Δ200 leu2Δ1 hpr1Δ::TRP1 pGPD-RNH1-HA::URA3 (pBB39)*	This study
YMB11246	*MATα ura3-52 lys2-801 ade2-101 trp1Δ63 his3Δ200 leu2Δ1*	This study
YMB11247	*MATα ura3-52 lys2-801 ade2-101 trp1Δ63 his3Δ200 leu2Δ1 hpr1Δ::TRP1*	This study
YMB11248	*MATα ura3-52 lys2-801 ade2-101 trp1Δ63 his3Δ200 leu2Δ1 hpr1Δ::TRP1 CEN-HPR1::URA3 (pMB1979)*	This study
YMB11251	*MATα ura3-52 lys2-801 ade2-101 trp1Δ63 his3-Δ200 leu2Δ1 hpr1Δ::TRP1 CFIII (CEN3L.YPH278) HIS3 SUP11 CEN-HPR1::URA3 (pMB1979)*	This study
KBY6380	*MATa trp1Δ63 ura3-52 his3 lys2 SPC42mCherry::NAT Ndc80-GFP::KAN*	Kerry Bloom, University of North Carolina, Chapell Hill, NC
KBY6432	*MATa trp1Δ63 ura3-52 his3 lys2 SPC42mCherry::NAT Ndc80-GFP::KAN hpr1Δ::HIS3*	This study
YMB11206	*MATα ura3-52 lys2-801 ade2-101 trp1Δ63 his3-Δ200 leu2Δ1 CFIII (CEN3L.YPH278) HIS3 SUP11 URA3-Vector (pRS426)*	This study
YMB11207	*MATα ura3-52 lys2-801 ade2-101 trp1Δ63 his3-Δ200 leu2Δ1 CFIII (CEN3L.YPH278) HIS3 SUP11 pGPD-RNH1-HA::URA3 (pBB39)*	This study
YMB11208	*MATα ura3-52 lys2-801 ade2-101 trp1Δ63 his3-Δ200 leu2Δ1 hpr1Δ::TRP1 CFIII (CEN3L.YPH278) HIS3 SUP11 URA3-Vector (pRS426)*	This study
YMB11209	*MATα ura3-52 lys2-801 ade2-101 trp1Δ63 his3-Δ200 leu2Δ1 hpr1Δ::TRP1 CFIII (CEN3L.YPH278) HIS3 SUP11 pGPD-RNH1-HA::URA3 (pBB39)*	This study
YMB11494	*MATa trp1Δ63 ura3-52 his3 lys2 SPC42mCherry::NAT Ndc80-GFP::KAN URA3-Vector (pRS426)*	This study
YMB11495	*MATa trp1Δ63 ura3-52 his3 lys2 SPC42mCherry::NAT Ndc80-GFP::KAN pGPD-RNH1-HA::URA3 (pBB39)*	This study
YMB11496	*MATa trp1Δ63 ura3-52 his3 lys2 SPC42mCherry::NAT Ndc80-GFP::KAN hpr1Δ::HIS3 URA3-Vector (pRS426)*	This study
YMB11497	*MATa trp1Δ63 ura3-52 his3 lys2 SPC42mCherry::NAT Ndc80-GFP::KAN hpr1Δ::HIS3 pGPD-RNH1-HA::URA3 (pBB39)*	This study

TABLE 1: Budding yeast strains, plasmids, and primers used in this study.

(Continues)

Plasmids			
Plasmid	**Description**		**Reference**
pBB39	*pGPD-RNH1-HA::URA3, 2-μ*		Bak *et al.*, 2013
pRS426	*URA3 Vector, 2-μ*		Christianson *et al.*, 1992
pMB1979	*CEN-HPR1::URA3*		Dharmacon
Primers			
Locus	**Forward (5′–3′)**	**Reverse (5′ –3′)**	**Reference**
CEN1	CTCGATTTGCATAAGTGTGCC	GTGCTTAAGAGTTCTGTACCAC	Choy *et al.*, 2011
CEN3	GATCAGCGCCAAACAATATGG	AACTTCCACCAGTAAACGTTTC	Paul Megee, Oakland University, Rochester, MI
CEN6	ACCTTGAAGACTATATTTCTTTT CATCACGTG	GGTCGTCCAATATCATCGTAAAC-GTG	John Choy, National Cancer Institute, Bethesda, MD (Basrai lab)
CEN7	AAGAGCTTCGATAAATTTGAAAAT-TAATTGTACTAC	CCTTGCATTATAATTATCCAA TACTTTGTCGTC	John Choy, National Cancer Institute, Bethesda, MD (Basrai lab)
CEN8	CCTTGAATGTACAGCTCTAATTACA-CAC	GATAATGTCTTAACCAATTTT CTAAGTTCGGAAC	John Choy, National Cancer Institute, Bethesda, MD (Basrai lab)
ACT1	ACAACGAATTGAGAGTTGCCCCAG	AATGGCGTGAGGTAGAGAGAAACC	Crotti and Basrai, 2004
169K	CATTATCAATCCTTGCGTTTCA	GCTCGAGTAATACCGGAGTGTC	Costantino and Koshland, 2018
179K	AAAGCTTTGTTTGCGGTATGTT	CCCGGATTACAAAGTCACTACC	Costantino and Koshland, 2018
310K	TCTCGGAATTTATCATGACCCAT	AAACCCTGCACACATTTCGT	Laloraya *et al.*, 2000
ADR1	AAGCCAGATAGCGGCAACT	CACTCACAGCTGGCATTAACA	Ciftci-Yilmaz *et al.*, 2018
GAL83	TTCATCGTCATCATCGTCGT	AAGGTCGTTTCCTGCACAAT	Ciftci-Yilmaz *et al.*, 2018
CSE4	CCATTTGCAAGGCTAGTGAAAG	CCAATAATCCTACCAGATACGC	Sultan Ciftci-Yilmaz, Lars Boeckmann, National Cancer Institute, Bethesda, MD (Basrai lab)
SCM3	ATGAAAACCAATAAGAAAATTTCTA-AAAG	TCCTTTTTGGTCTTCCGTTTTTCG	This study
TUB2	ATTGACGGCAATTGGCTCT	ACCAGTGCAAGAAAGCTTTTC	Carole Carter, National Cancer Institute, Bethesda, MD (Basrai lab)
SLD2	AGCTGAAAACATGGGAGCAT	TCGCCTTACCGTAAACTTGG	Ciftci-Yilmaz *et al.*, 2018
RRP12	CATTTCTTCTGGATTGGCTGA	ACATTGAGAGGCAGCTTGGT	Ciftci-Yilmaz *et al.*, 2018

TABLE 1: Budding yeast strains, plasmids, and primers used in this study. Continued

to the manufacturer's instruction (Cat# 74106; Qiagen). DNase-treated RNA was reverse transcribed using the Access RT-PCR System (Promega Corporation, Madison, WI) in a 10-μl reaction with the primers listed in Table 1. Expression levels of *CEN*s (*CEN1*, *CEN3*, *CEN6*, *CEN7*, and *CEN8*) and genes (*ACT1*, *ADR1*, *CSE4*, *GAL83*, *RRP12*, *SCM3*, *SLD2*, and *TUB2)* were determined by real-time qPCR using 7500 Fast SYBR Green Master Mix (Applied Biosystems). RNA samples processed through the RT step without reverse transcriptase enzyme were used as negative controls. The C_T values, which denote the number of PCR cycles needed to cross the threshold fluorescence in the amplification curve ($t_{½}$ of the exponential region of amplification), were determined for each sample, and the corresponding LOG transcription was deduced from a standard curve (Supplemental Figure S7) prepared under identical conditions based on quantitation of a 323 base pair product with increasing amounts (10^2, 10^3, 10^4, 10^5, and 10^6 copies) of control mRNA (Promega Corporation). For *CEN* lncRNA experiments, the relative fold changes were calculated after normalization to the G1 cells, where G1 was set to a value of 1. *ACT1*, which is expressed constitutively with transcription levels similar in G1- and S-phase, was used as a positive control. Three independent biological replicates for each sample were performed, and the statistical significance of the data was determined as described previously (Ling and Yuen, 2019).

Microscopy and kinetochore biorientation assay

Yeast cells containing the SPB protein Spc42-mCherry and the outer kinetochore protein Ndc80-GFP were imaged at 25°C on a Nikon Eclipse Ti wide-field inverted microscope with a 100×Apo total internal reflection fluorescence 1.49 numerical aperture objective (Nikon, Melville, NY) and Andor Clara charge-coupled device camera (Andor, South Windsor, CT). Images were acquired using Nikon Elements imaging software. Images were taken in transilluminated light and GFP and RFP fluorescence illumination. Metaphase spindles are in the length range of 1.4–1.7 μm.

Dilution plating assays

WT and *hpr1*Δ strains were grown in YPD medium at 25°C, and cell suspensions were prepared in water to obtain an $OD_{600} = 2.0$. Then 5 μl of the cell suspension was plated on YPD plates in serial fivefoldl

dilutions. Cells were incubated on plates at 25° and 37°C to examine the temperature sensitivity phenotype. Benomyl sensitivity was determined at 25°C on YPD plates, with or without 10 μg/ml benomyl (Cat# 17804-35-2; Aldrich Chemicals).

Chromosome transmission fidelity assay

The frequency of chromosome segregation was measured by a colony color assay in which the loss of a reporter CF results in red-colored sectors in an otherwise white colony (Spencer *et al.*, 1990). WT and *hpr1*Δ strains containing the CF were grown to early logarithmic phase in medium selective for the CF and the plasmids being used. Cells were then plated on synthetic dextrose agar medium with limiting adenine at 25°C. The frequency of CF loss represents the number of colonies that were at least half red (indicative of CF loss in the first cell division) over the total number of colonies counted. About 1000 colonies from three independent transformants were examined for each strain.

ACKNOWLEDGMENTS

We appreciate technical support for ssDNA mapping from Jie Peng. We thank Andres Aguilera, Sue Biggins, Jennifer Gerton, and Vincent Guacci for strains and plasmids; Kathy McKinnon of the National Cancer Institute Vaccine Branch FACS Core for technical assistance; and the members of the Basrai laboratory for helpful discussions. P.K.M. and M.A.B. were supported by the Intramural Research Program of the National Cancer Institute, National Institutes of Health (NIH). E. Y. and K. B. were supported by NIH grant R37 GM32238; W. F. and A. C. were supported by NIH grant GM118799-01A1.

REFERENCES

Aguilera A, Klein HL (1990). HPR1, a novel yeast gene that prevents intrachromosomal excision recombination, shows carboxy-terminal homology to the Saccharomyces cerevisiae TOP1 gene. Mol Cell Biol 10, 1439–1451.

Allison DF, Wang GG (2019). R-loops: formation, function, and relevance to cell stress. Cell Stress 3, 38–46.

Andronov L, Ouararhni K, Stoll I, Klaholz BP, Hamiche A (2019). CENP-A nucleosome clusters form rosette-like structures around HJURP during G1. Nat Commun 10, 4436.

Au WC, Crisp MJ, DeLuca SZ, Rando OJ, Basrai MA (2008). Altered dosage and mislocalization of histone H3 and Cse4p lead to chromosome loss in Saccharomyces cerevisiae. Genetics 179, 263–275.

Bakhoum SF, Swanton C (2014). Chromosomal instability, aneuploidy, and cancer. Front Oncol 4, 161.

Balk B, Maicher A, Dees M, Klermund J, Luke-Glaser S, Bender K, Luke B (2013). Telomeric RNA-DNA hybrids affect telomere-length dynamics and senescence. Nat Struct Mol Biol 20, 1199–1205.

Barra V, Fachinetti D (2018). The dark side of centromeres: types, causes and consequences of structural abnormalities implicating centromeric DNA. Nat Commun 9, 4340.

Bloom K, Costanzo V (2017). Centromere structure and function. Prog Mol Subcell Biol 56, 515–539.

Camahort R, Li B, Florens L, Swanson SK, Washburn MP, Gerton JL (2007). Scm3 is essential to recruit the histone h3 variant cse4 to centromeres and to maintain a functional kinetochore. Mol Cell 26, 853–865.

Castellano-Pozo M, Santos-Pereira JM, Rondon AG, Barroso S, Andujar E, Perez-Alegre M, Garcia-Muse T, Aguilera A (2013). R loops are linked to histone H3 S10 phosphorylation and chromatin condensation. Mol Cell 52, 583–590.

Chan YA, Aristizabal MJ, Lu PY, Luo Z, Hamza A, Kobor MS, Stirling PC, Hieter P (2014). Genome-wide profiling of yeast DNA:RNA hybrid prone sites with DRIP-chip. PLoS Genet 10, e1004288.

Chavez S, Aguilera A (1997). The yeast HPR1 gene has a functional role in transcriptional elongation that uncovers a novel source of genome instability. Genes Dev 11, 3459–3470.

Chavez S, Beilharz T, Rondon AG, Erdjument-Bromage H, Tempst P, Svejstrup JQ, Lithgow T, Aguilera A (2000). A protein complex containing Tho2, Hpr1, Mft1 and a novel protein, Thp2, connects transcription elongation with mitotic recombination in Saccharomyces cerevisiae. EMBO J 19, 5824–5834.

Chavez S, Garcia-Rubio M, Prado F, Aguilera A (2001). Hpr1 is preferentially required for transcription of either long or G+C-rich DNA sequences in Saccharomyces cerevisiae. Mol Cell Biol 21, 7054–7064.

Cheeseman IM, Anderson S, Jwa M, Green EM, Kang J, Yates JR 3rd, Chan CS, Drubin DG, Barnes G (2002). Phospho-regulation of kinetochore-microtubule attachments by the Aurora kinase Ipl1p. Cell 111, 163–172.

Chen CF, Pohl TJ, Chan A, Slocum JS, Zakian VA (2019). Saccharomyces cerevisiae centromere RNA is negatively regulated by Cbf1 and its unscheduled synthesis impacts CenH3 binding. Genetics 213, 465–479.

Choy JS, Acuna R, Au WC, Basrai MA (2011). A role for histone H4K16 hypoacetylation in Saccharomyces cerevisiae kinetochore function. Genetics 189, 11–21.

Christianson TW, Sikorski RS, Dante M, Shero JH, Hieter P (1992). Multifunctional yeast high-copy-number shuttle vectors. Gene 110, 119–122.

Ciftci-Yilmaz S, Au WC, Mishra PK, Eisenstatt JR, Chang J, Dawson AR, Zhu I, Rahman M, Bilke S, Costanzo M, *et al.* (2018). A genome-wide screen reveals a role for the HIR histone chaperone complex in preventing mislocalization of budding yeast CENP-A. Genetics 210, 203–218.

Collins KA, Castillo AR, Tatsutani SY, Biggins S (2005). De novo kinetochore assembly requires the centromeric histone H3 variant. Mol Biol Cell 16, 5649–5660.

Costantino L, Koshland D (2018). Genome-wide map of R-loop-induced damage reveals how a subset of R-loops contributes to genomic instability. Mol Cell 71, 487–497.e483.

Crossley MP, Bocek M, Cimprich KA (2019). R-loops as cellular regulators and genomic threats. Mol Cell 73, 398–411.

Crotti LB, Basrai MA (2004). Functional roles for evolutionarily conserved Spt4p at centromeres and heterochromatin in Saccharomyces cerevisiae. EMBO J 23, 1804–1814.

Diaz-Ingelmo O, Martinez-Garcia B, Segura J, Valdes A, Roca J (2015). DNA topology and global architecture of point centromeres. Cell Rep 13, 667–677.

El Hage A, French SL, Beyer AL, Tollervey D (2010). Loss of topoisomerase I leads to R-loop-mediated transcriptional blocks during ribosomal RNA synthesis. Genes Dev 24, 1546–1558.

El Hage A, Webb S, Kerr A, Tollervey D (2014). Genome-wide distribution of RNA-DNA hybrids identifies RNase H targets in tRNA genes, retrotransposons and mitochondria. PLoS Genet 10, e1004716.

Fan HY, Cheng KK, Klein HL (1996). Mutations in the RNA polymerase II transcription machinery suppress the hyperrecombination mutant hpr1 delta of Saccharomyces cerevisiae. Genetics 142, 749–759.

Feng W, Collingwood D, Boeck ME, Fox LA, Alvino GM, Fangman WL, Raghuraman MK, Brewer BJ (2006). Genomic mapping of single-stranded DNA in hydroxyurea-challenged yeasts identifies origins of replication. Nat Cell Biol 8, 148–155.

Furuyama S, Biggins S (2007). Centromere identity is specified by a single centromeric nucleosome in budding yeast. Proc Natl Acad Sci USA 104, 14706–14711.

Furuyama T, Henikoff S (2009). Centromeric nucleosomes induce positive DNA supercoils. Cell 138, 104–113.

Gan W, Guan Z, Liu J, Gui T, Shen K, Manley JL, Li X (2011). R-loop-mediated genomic instability is caused by impairment of replication fork progression. Genes Dev 25, 2041–2056.

Garcia-Pichardo D, Canas JC, Garcia-Rubio ML, Gomez-Gonzalez B, Rondon AG, Aguilera A (2017). Histone mutants separate R loop formation from genome instability induction. Mol Cell 66, 597–609.e595.

Gomez-Gonzalez B, Felipe-Abrio I, Aguilera A (2009). The S-phase checkpoint is required to respond to R-loops accumulated in THO mutants. Mol Cell Biol 29, 5203–5213.

Groh M, Gromak N (2014). Out of balance: R-loops in human disease. PLoS Genet 10, e1004630.

Haase J, Mishra PK, Stephens A, Haggerty R, Quammen C, Taylor RM 2nd, Yeh E, Basrai MA, Bloom K (2013). A 3D map of the yeast kinetochore reveals the presence of core and accessory centromere-specific histone. Curr Biol 23, 1939–1944.

Henikoff S, Furuyama T (2010). Epigenetic inheritance of centromeres. Cold Spring Harb Symp Quant Biol 75, 51–60.

Heun P, Erhardt S, Blower MD, Weiss S, Skora AD, Karpen GH (2006). Mislocalization of the Drosophila centromere-specific histone CID promotes formation of functional ectopic kinetochores. Dev Cell 10, 303–315.

Hill A, Bloom K (1987). Genetic manipulation of centromere function. Mol Cell Biol 7, 2397–2405.

Huang CC, Chang KM, Cui H, Jayaram M (2011). Histone H3-variant Cse4-induced positive DNA supercoiling in the yeast plasmid has implications for a plasmid origin of a chromosome centromere. Proc Natl Acad Sci USA 108, 13671–13676.
Huertas P, Aguilera A (2003). Cotranscriptionally formed DNA:RNA hybrids mediate transcription elongation impairment and transcription-associated recombination. Mol Cell 12, 711–721.
Huertas P, Garcia-Rubio ML, Wellinger RE, Luna R, Aguilera A (2006). An hpr1 point mutation that impairs transcription and mRNP biogenesis without increasing recombination. Mol Cell Biol 26, 7451–7465.
Hyland KM, Kingsbury J, Koshland D, Hieter P (1999). Ctf19p: a novel kinetochore protein in Saccharomyces cerevisiae and a potential link between the kinetochore and mitotic spindle. J Cell Biol 145, 15–28.
Jin Q, Trelles-Sticken E, Scherthan H, Loidl J (1998). Yeast nuclei display prominent centromere clustering that is reduced in nondividing cells and in meiotic prophase. J Cell Biol 141, 21–29.
Jin QW, Fuchs J, Loidl J (2000). Centromere clustering is a major determinant of yeast interphase nuclear organization. J Cell Sci 113(Pt 11), 1903–1912.
Joglekar AP, Salmon ED, Bloom KS (2008). Counting kinetochore protein numbers in budding yeast using genetically encoded fluorescent proteins. Methods Cell Biol 85, 127–151.
Kabeche L, Nguyen HD, Buisson R, Zou L (2018). A mitosis-specific and R loop-driven ATR pathway promotes faithful chromosome segregation. Science 359, 108–114.
Kastenmayer JP, Lee MS, Hong AL, Spencer FA, Basrai MA (2005). The C-terminal half of Saccharomyces cerevisiae Mad1p mediates spindle checkpoint function, chromosome transmission fidelity and CEN association. Genetics 170, 509–517.
Laloraya S, Guacci V, Koshland D (2000). Chromosomal addresses of the cohesin component Mcd1p. J Cell Biol 151, 1047–1056.
Lawrimore J, Bloom K (2019). The regulation of chromosome segregation via centromere loops. Crit Rev Biochem Mol Biol 54, 352–370.
Lawrimore J, Bloom KS, Salmon ED (2011). Point centromeres contain more than a single centromere-specific Cse4 (CENP-A) nucleosome. J Cell Biol 195, 573–582.
Lawrimore J, Doshi A, Friedman B, Yeh E, Bloom K (2018). Geometric partitioning of cohesin and condensin is a consequence of chromatin loops. Mol Biol Cell 29, 2737–2750.
Ling YH, Yuen KWY (2019). Point centromere activity requires an optimal level of centromeric noncoding RNA. Proc Natl Acad Sci USA 116, 6270–6279.
Liu Y, Su H, Zhang J, Liu Y, Feng C, Han F (2020). Back-spliced RNA from retrotransposon binds to centromere and regulates centromeric chromatin loops in maize. PLoS Biol 18, e3000582.
Livak KJ, Schmittgen TD (2001). Analysis of relative gene expression data using real-time quantitative PCR and the 2(-Delta Delta C(T))Method. Methods 25, 402–408.
Luna R, Rondon AG, Perez-Calero C, Salas-Armenteros I, Aguilera A (2019). The THO complex as a paradigm for the prevention of cotranscriptional R-loops. Cold Spring Harb Symp Quant Biol 84, 105–114.
Ma L, Ho K, Piggott N, Luo Z, Measday V (2012). Interactions between the kinetochore complex and the protein kinase A pathway in Saccharomyces cerevisiae. G3 (Bethesda) 2, 831–841.
McKinley KL, Cheeseman IM (2016). The molecular basis for centromere identity and function. Nat Rev Mol Cell Biol 17, 16–29.
Miller MP, Evans RK, Zelter A, Geyer EA, MacCoss MJ, Rice LM, Davis TN, Asbury CL, Biggins S (2019). Kinetochore-associated Stu2 promotes chromosome biorientation in vivo. PLoS Genet 15, e1008423.
Mishra PK, Au WC, Choy JS, Kuich PH, Baker RE, Foltz DR, Basrai MA (2011). Misregulation of Scm3p/HJURP causes chromosome instability in Saccharomyces cerevisiae and human cells. PLoS Genet 7, e1002303.
Mishra PK, Basrai MA (2019). Protein kinases in mitotic phosphorylation of budding yeast CENP-A. Curr Genet 65, 1325–1332.
Mishra PK, Baum M, Carbon J (2007). Centromere size and position in Candida albicans are evolutionarily conserved independent of DNA sequence heterogeneity. Mol Genet Genomics 278, 455–465.
Mishra PK, Ciftci-Yilmaz S, Reynolds D, Au WC, Boeckmann L, Dittman LE, Jowhar Z, Pachpor T, Yeh E, Baker RE, *et al*. (2016). Polo kinase Cdc5 associates with centromeres to facilitate the removal of centromeric cohesin during mitosis. Mol Biol Cell 27, 2286–2300.
Mishra PK, Guo J, Dittman LE, Haase J, Yeh E, Bloom K, Basrai MA (2015). Pat1 protects centromere-specific histone H3 variant Cse4 from Psh1-mediated ubiquitination. Mol Biol Cell 26, 2067–2079.
Mishra PK, Ottmann AR, Basrai MA (2013). Structural integrity of centromeric chromatin and faithful chromosome segregation requires Pat1. Genetics 195, 369–379.
Mishra PK, Thapa KS, Chen P, Wang S, Hazbun TR, Basrai MA (2018). Budding yeast CENP-A(Cse4) interacts with the N-terminus of Sgo1 and regulates its association with centromeric chromatin. Cell Cycle 17, 11–23.
Mizuguchi G, Xiao H, Wisniewski J, Smith MM, Wu C (2007). Nonhistone Scm3 and histones CenH3-H4 assemble the core of centromere-specific nucleosomes. Cell 129, 1153–1164.
Ng TM, Waples WG, Lavoie BD, Biggins S (2009). Pericentromeric sister chromatid cohesion promotes kinetochore biorientation. Mol Biol Cell 20, 3818–3827.
Ohkuni K, Kitagawa K (2012). Role of transcription at centromeres in budding yeast. Transcription 3, 193–197.
Pearson CG, Yeh E, Gardner M, Odde D, Salmon ED, Bloom K (2004). Stable kinetochore-microtubule attachment constrains centromere positioning in metaphase. Curr Biol 14, 1962–1967.
Ranjitkar P, Press MO, Yi X, Baker R, MacCoss MJ, Biggins S (2010). An E3 ubiquitin ligase prevents ectopic localization of the centromeric histone H3 variant via the centromere targeting domain. Mol Cell 40, 455–464.
Rondon AG, Aguilera A (2019). R-loops as promoters of antisense transcription. Mol Cell 76, 529–530.
Santos-Pereira JM, Aguilera A (2015). R loops: new modulators of genome dynamics and function. Nat Rev Genet 16, 583–597.
Santos-Rosa H, Aguilera A (1994). Increase in incidence of chromosome instability and non-conservative recombination between repeats in Saccharomyces cerevisiae hpr1 delta strains. Mol Gen Genet 245, 224–236.
Sharma AB, Dimitrov S, Hamiche A, Van Dyck E (2019). Centromeric and ectopic assembly of CENP-A chromatin in health and cancer: old marks and new tracks. Nucleic Acids Res 47, 1051–1069.
Spencer F, Gerring SL, Connelly C, Hieter P (1990). Mitotic chromosome transmission fidelity mutants in Saccharomyces cerevisiae. Genetics 124, 237–249.
Stirling PC, Chan YA, Minaker SW, Aristizabal MJ, Barrett I, Sipahimalani P, Kobor MS, Hieter P (2012). R-loop-mediated genome instability in mRNA cleavage and polyadenylation mutants. Genes Dev 26, 163–175.
Stoler S, Keith KC, Curnick KE, Fitzgerald-Hayes M (1995). A mutation in CSE4, an essential gene encoding a novel chromatin-associated protein in yeast, causes chromosome nondisjunction and cell cycle arrest at mitosis. Genes Dev 9, 573–586.
Stoler S, Rogers K, Weitze S, Morey L, Fitzgerald-Hayes M, Baker RE (2007). Scm3, an essential Saccharomyces cerevisiae centromere protein required for G2/M progression and Cse4 localization. Proc Natl Acad Sci USA 104, 10571–10576.
Tan-Wong SM, Dhir S, Proudfoot NJ (2019). R-loops promote antisense transcription across the mammalian genome. Mol Cell 76, 600–616.e606.
Wells JP, White J, Stirling PC (2019). R loops and their composite cancer connections. Trends Cancer 5, 619–631.
Yeh E, Haase J, Paliulis LV, Joglekar A, Bond L, Bouck D, Salmon ED, Bloom KS (2008). Pericentric chromatin is organized into an intramolecular loop in mitosis. Curr Biol 18, 81–90.
Yoder TJ, McElwain MA, Francis SE, Bagley J, Muller EG, Pak B, O'Toole ET, Winey M, Davis TN (2005). Analysis of a spindle pole body mutant reveals a defect in biorientation and illuminates spindle forces. Mol Biol Cell 16, 141–152.
Zenklusen D, Vinciguerra P, Wyss JC, Stutz F (2002). Stable mRNP formation and export require cotranscriptional recruitment of the mRNA export factors Yra1p and Sub2p by Hpr1p. Mol Cell Biol 22, 8241–8253.